1-29-2009

Laboratory evaluation of cracking in asphalt concrete

Evan Michael Casey Kias

Evan M.C. Kias

Candidate

Civil Engineering

Department

This thesis is approved, and it is acceptable in quality and form for publication on microfilm:

Approved by the Thesis Committee:

Rafi Tarefder 11/12/08

, Chairperson

11/12/08

11/12/08

Accepted:

Dean, Graduate School

NOV 17 2008

Date

Laboratory Evaluation of Cracking in Asphalt Concrete

By

Evan M. C. Kias

B.S., Physics and Astronomy, University of New Mexico, 2005

THESIS

Submitted in Partial Fulfillment of the
Requirements for the Degree of

MASTER OF SCIENCE
Civil Engineering

The University of New Mexico
Albuquerque, New Mexico

December 2008

DEDICATION

This work is dedicated to my family: Michael, Susan, and Lauren, whom have nurtured me along my path in realizing this goal.

Thank you, the value of your support is immeasurable.

ACKNOLEDGEMENTS

I would also like to thank the following for the various roles they have played:

Thank you to my peers who have helped me along the way.

My instructors at UNM, for aiding me to learn to utilize my strengths and identify my weaknesses.

The staff at UNM Civil Engineering, for their attention amongst a sea of tasks.

Mr. Lary Lenke, for forging my pathway and helping me to begin my career as a civil engineer.

Members of my thesis committee: Percy Ng and John Stormont for their valuable perspectives and advice.

Dr. Tarefder, for the countless hours of tutelage. The lessons and skills learned during my stay are invaluable.

Laboratory Evaluation of Cracking in Asphalt Concrete

By

Evan M. C. Kias

ABSTRACT OF THESIS

Submitted in Partial Fulfillment of the
Requirements for the Degree of

MASTER OF SCIENCE
Civil Engineering

The University of New Mexico
Albuquerque, New Mexico

December 2008

LABORATORY EVALUATION OF

CRACKING IN ASPHALT CONCRETE

By

Evan M. C. Kias

B.S., Physics and Astronomy, University of New Mexico, 2005

M.S., Civil Engineering, University of New Mexico, 2008

ABSTRACT

Cracking is one of the major distresses in asphalt concrete leading to high maintenance and rehabilitation costs throughout the nation's pavement infrastructure. Asphalt concrete is a three phase, heterogeneous composite consisting of aggregate, mastic, and air voids. Crack initiation, crack path and propagation are not well understood in asphalt concrete. This thesis work presents testing and analysis of cracking in semi-circular notched asphalt concrete samples in three point bending. Load and crack width data at different locations of the sample were captured in real time using Linear Variable Differential Transformers (LVDTs). Crack initiation, path, and velocity are examined with varying notch tip location, mixture type, void content, and moisture conditioning. Crack path is further examined by means of laboratory testing on the mastic and interface phases of asphalt concrete.

TABLE OF CONTENTS

LIST OF TABLES

LIST OF FIGURES

CHAPTER 1

Introduction

1.1 Introduction

Cracking is one of the major distresses of Hot Mix Asphalt (HMA) pavements. Cracks in HMA provide a pathway for water, which can lead to damage in the form of binder stripping and softening of the mastic. This type of damage contributes to a decrease in HMA pavement's serviceability, which in turn increases pavement maintenance and reconstruction costs. HMA pavement constitutes a sizeable portion of the United States Department of Transportation's annual expenditure on construction and rehabilitation of the country's pavement infrastructure. This study focuses on laboratory characterization of cracking in asphalt concrete.

Several test methods have been developed to study the cracking behavior in HMA under different sample geometries, loading configurations, and material properties (Aglan et al. 1994, Bynum et al. 1973, Dongre et al. 1989, Mull et al. 2002). In most tests, a notch has been introduced into the sample so that the crack will initiate at the notch (Molenaar et al. 2002, Wagoner et al. 2005a, Wagoner et al. 2005b, Wu et al. 2005). In many of these studies, linear elastic fracture mechanics and elastic plastic fracture mechanics principles have been applied to test observations to better characterize material response to stress and strain (Hofman et al. 2003, Mull et al. 2002, Zhang et al. 2001). Recently, crack propagation is observed using a video recorder and crack length is measured at different times using a standardized ruler (Hofman et al. 2003). In this study, instead of a video technique, linear variable differential transducers are used to determine the crack

propagation within the sample. This is the first time such a method has been implemented to determine crack initiation, propagation, and velocity in the laboratory.

HMA has three phases: interface, aggregate, and mastic. The interface is defined as the surface that is the boundary between the binder, or mastic, and the aggregate. The aggregate consists of coarse particulate matter that is coated with binder and forms the load-bearing skeleton of the HMA. The mastic is a the mixture of fine aggregate passing the #200 sieve and asphalt binder, which is a viscoelastic composite that has adhesive and cohesive properties capable of withstanding tensile forces. Cracks can initiate and propagate through any of these three phases. Understanding how cracks initiate in each of the phases of HMA is pivotal to accurately predicting cracking in the service pavements. Because an accurate prediction of crack initiation and propagation aids in the design and maintenance of asphalt pavement structures. Parameters such as the crack width and cracking loads can be used to describe the remaining life of the service pavements. To examine crack initiation point, the HMA samples are fabricated in this study to have a crack tip in the interface, aggregate, and mastic. In essence, rectangular notches having a tip on one of these three phases are cut into semi-circular HMA specimens. The initiation of a crack may depend on the notch size and length (Mull et al. 2002). In this study, notch size and length are kept constant for simplicity. The notch serves as a predetermined crack initiation point from where crack propagation is observed.

As a crack propagates in asphalt concrete the crack has two measurable quantities that can be observed: the crack width and the crack length. This study captures the crack width in real time at three defined locations away from the notch tip using Linear Variable Differential Transducers (LVDTs). The crack length is measured using the times history of the LVDT data. Crack propagation and initiation can be observed through several mixes to have a heneral understanding. In this study, three mixes are evaluated. Specimens are compacted using a Superpave gyratory compactor in the laboratory. Asphalt specimens are cut and notched using a laboratory saw. The notched specimens are tested under monotonic loading in strain-controlled mode and crack width are recorded in real time. Crack path in each specimen is observed and compared to the aggregate gradation.

Properties of HMA concrete such as air voids or density, moisture damage condition, or aggregate gradation may affect crack initiation and crack propagation. Performance tests of asphalt concrete have generally been conducted on specimens within a narrow band of air void contents (Jacobs et al. 1995, Van de Ven et al. 1997, Zhang et al 2002). The effects of air void content on crack initiation propagation can be realized by utilizing specimens prepared at varying void ratios. Currently a standard procedure AASHTO T283 is used to conduct a moisture damage assessment on asphalt concrete mixes of various types. This procedure involves a freeze thaw process analogous to moisture conditions and temperature changes that occur in the field. Both the moisture conditioned and dry cylindrical specimens are loaded in diametral compression and peak loads are compared.

1.2 Objectives

The main objective of this study is to characterize crack initiation and propagation in asphalt concrete. The specific objectives are to:

1. Characterize crack initiation and propagation through asphalt concrete in laboratory experiments.
2. Derive a set of parameters based on laboratory load versus crack results and determine the effects of mixture properties such as notch location, moisture condition, void ratio, and mix type on crack initiation and propagation using these parameters.
3. Evaluate possible crack pathways by micro-mechanical testing of the phases of asphalt concrete in tension, compression, and shear.

CHAPTER 2

Literature Review

2.1 Laboratory Testing and Fracture Mechanics

Cracking of asphalt concrete has been extensively researched by means of laboratory testing. However, the fracture of asphalt concrete did not become popular topic of research until the realization of the problem of reflective cracking of asphalt overlays. Recently, many tests have been examined with the goal to determine the general fracture properties of asphalt concrete. The following section describes the recent advancements in the study of crack initiation and propagation in asphalt concrete (AC):

Some researchers have tested AC under the assumption that it behaves as a linear elastic material (Herrin and Bhagat 1968, Majidzadeh, et al. 1969, and Majidzadeh, et al. 1971). Two parameters generated from linear elastic fracture mechanics that are widely used in the characterization of fracture in asphalt concrete are the energy release rate, G, and the fracture toughness, K_C. Some researchers have idealized the visco-elastic behavior of asphalt concrete as non–linear elastic and applied elastic–plastic fracture mechanics (EPFM) concepts to the fracture (Rice 1968). In 1985, Abdulshafi and Majidzadeh used the critical strain energy release rate, or J–integral, to characterize notched disc shaped samples. The J-Integral can be determined in the laboratory using similar samples of varying notch lengths (Anderson 2005).

2.2 Specimen Geometry

It is known that specimen shape and size can affect the outcome of a material fracture

test. Over the last few decades, the sample geometry and the testing procedure have evolved to better determine fracture properties in accordance with fracture mechanics principles. For example, sample geometry and support have changed to better represent field conditions. The following paragraphs describe these pertinent and recent advances:

There are four basic sample geometries that can be considered for the study of fracture in asphalt concrete: the direct tension sample, the single-edge notched beam sample, the disc-shaped compact tension sample, and the semi-circular bending specimen. These sample geometries are shown in Figure 2.1. The direct tension specimen D(T) is a beam shaped specimen that is notched through the width of both lengths of the specimen (Jacobs et al 1995). The dimensions for the sample used in Jacobs et al. (1996) are 2 in x 2 in x 6 in (50 mm x 50 mm x 150 mm). This specimen is loaded in tension uniaxially along the longest dimension. At failure, a crack grows from each notch tip towards the center of the specimen, where the cracks from each notch meet. Test results from this specimen are highly dependent upon the fabrication and test setup. If the notches are cut into the specimen symmetrically, a difference in stress intensity at opposing notch tips can lead to different crack growth rates from each crack. Subsequently, an unintended moment may be imposed on the sample that results in mixed mode loading in the fracture zone. Mixed mode loads occur when combinations of mode I, mode II, or mode III loading are present. Also, this specimen geometry is dependent upon gluing the ends of the sample to the loading apparatus, which is time consuming and prone to failure. For these reasons, studies applying this specimen geometry are limited in number.

The single-edge notched beam SE(B) specimen shown in Figure 2.1(b) is a beam shaped specimen with a rectangular cross section (Wagoner et al. 2005a). The typical size of the beam is approximately 375 mm long by 100 mm tall by 75 mm wide. The beam is notched in the center of the length through the width. This specimen is advantageous to use in fracture studies because of its potentially large fracture area. Also movement of the notch along the length of the sample allows for investigation into mixed mode loading. However, obtaining field samples of single-edge notched beam samples is difficult.

The disk-shaped compact tension DC(T) specimen is shown in Figure 2.1(c). The DC(T) sample is sliced from a Superpave Gyratory Compactor (SGC) sample or from a cylindrical core taken from an in service pavement (Wagoner et al. 2005). A flat edge is sawn from circular edge of the core so that a notch may be cut to facilitate fracture. The sample is loaded in direct tension by means of supports through the holes drilled on each side of the notch. The DC(T) sample is attractive for research purposes because it can be fabricated from field cores. The sample also allows for a large fracture area, albeit less than the SE(B) sample, which reduces the effects of specimen geometry on crack initiation and propagation. The downside to this sample is the possible deviation of the crack from the line of symmetry. This is due to the incorrect placement of the support holes. Since this is a process that requires precision during fabrication, dependency of test results on sample preparation is high.

The semi-circular bending SC(B) specimen is shown in Figure 2.1(d). The SC(B) specimen is fabricated by slicing a cylindrical asphalt sample in half and notching the flat edge. Since this specimen may also be fabricated from field cores, it provides an accurate representation of field conditions. The specimen is loaded in a three point bending configuration, so the asymmetric loading problem associated with the D(T) sample is eliminated. The semi-circular shape allows for more specimens to be produced from a single core, but reduces the initial ligament length and therefore the fracture area. It is believed that as research into the effects of specimen size, shape then the SC(B) specimen will prove to be the most efficient specimen for fracture testing because of the number of samples obtainable from a single field core.

To date, most investigations into the fracture properties of asphalt concrete have been conducted using the SE(B) specimen (Dongre et al. 1989, Jacobs et al. 1995, Mobasher et al. 1997, Wagoner et al. 2005a). Lately there has been a push to use the DC(T) and SC(B) specimens due to their ability to be fabricated from field cores.

2.3 Fracture Studies

The text above has mentioned several valuable studies of fracture in asphalt concrete using the SE(B), DC(T), and SC(B) specimens. A standardized test procedure has yet to be defined that characterizes the fracture properties of an asphalt mixture. Many of the studies explored fracture parameters that sufficiently quantifies an asphalt mixture's performance related to cracking.

Dongre et al (1989) studied the fracture in asphalt concrete by means of both LEFM and EPFM. The LEFM technique lead to the calculation of K_{IC}, while the EPFM technique lead to the calculation of J_{IC}. The testing procedure involved loading a SE(B) specimen using a loading rate of 1.5 lbs/sec until fracture. Specimens were compacted to an air void ratio of 5±0.5% using one common aggregate gradation and twelve different asphalt binder types. The specimens were tested at five different temperatures ranging from 60°F (16°C) to -5°F (-20°C). The authors concluded that K_{IC} showed no sensitivity to the test variables while J_{IC} showed promise as a fracture parameter within the temperature range examined. In particular, J_{IC} was sensitive to both the source and hardness of the asphalt type. Furthermore, this study helped to demonstrate the unreliability of LEFM in characterizing the fracture behavior of asphalt concrete.

Aglan et al. (1994) examined the effect of styrene-butadiene-styrene (SBS) block copolymers on the behavior of asphalt mixtures using the beam shaped specimen. An unnotched specimen was tested by Aglan and his colleagues under static load to determine ultimate strength and the elastic modulus of the mixture with different percentages of SBS added to the binder. Then a cyclic test was conducted on a notched beam to determine the specific energy of damage by way of the modified crack layer model (Aglan 1993). The specific energy of damage is a coefficient in the linear relationship between the energy release rate normalized by the notch length and the change in work normalized by the increase in crack length per cycle times the notch length. Aglan's study showed that the ultimate strength in the unnotched static test

increased with increased polymer percentage, and the specific energy of damage increased with increased polymer percentage.

Jacobs et al. (1996) conducted an investigation on cracking in asphalt concrete in. LEFM concepts were utilized to study cracking using Paris's law of crack propagation (Paris and Erdogan 1963):

$$\frac{dc}{dN} = AK^n \qquad \text{(eq. 1)}$$

$$\begin{aligned} \textit{where: } c &= \textit{crack length} \\ N &= \textit{number of load cycles} \\ K &= \textit{stress} \text{ intensity factor} \\ A, n &= \textit{material parameters} \end{aligned}$$

Jacobs and colleagues conducted cyclic and static load tests on the DC(T) specimen to determine the material parameters. By inputting COD data into a finite element model the stress intensity factor can be calculated numerically. Also, the crack length was determined with the assumption that the relationship between crack length and the COD is linear. Jacobs's study concluded with some trends in the material parameters suggesting that less air voids, higher filler percentage, and higher binder content increased the exponent, n, resulting in faster crack propagation.

Krans et al. (1996) compared the SCB specimen to other the other possible crack investigation geometries: DTS, center cracked tension sample CC(T), indirect tension sample I(T), and SE(B) in three and four point bending. Krans's paper uses pre-existing laboratory studies that utilized the above speciemens to show that the SC(B) specimen is

a viable candidate for quality control of mix and pavement design and a valuable tool for studying cracking in asphalt concrete. First the authors describe the setbacks to other geometries, and then shows test results for cyclic and static load tests on both unnotched and notched SCB specimens. The paper refers to cyclic testing of SC(B) samples in order to determine cycles to failure, N_f, and the Paris law (eq. 1) material parameters, A and n. A finite element model of the SC(B) specimen is coupled with static tests of notched samples to determine the stress intensity factor for mode I loading, K_C. While the study supplies a method for calculating K_C, the authors warn that the application of LEFM is limited to low temperature cracking.

In response to the inaccuracy of LEFM in describing crack initiation and propagation, Mobasher et al. used nonlinear fracture parameters to compare asphalt concrete to a concrete with rubber infused binder (Mobasher et al. 1997). Cyclic testing was conducted on SENB specimens to determine mixture fracture properties based on a compliance method and the resistance curve (R-curve). The study showed that a nonlinear stress intensity factor with added compliance and inelastic terms exhibited sensitivity to binder content and temperature of the test mixes, but not the difference in binder type. Although the change in fracture property due to binder type was demonstrated by the toughness, G_f, which is also a parameter independent of the linearity of the material. The R-curve performed well in differentiating between mixes of varying binder content.

Mull et al. (2002) also used the J-integral concept to evaluate modified asphalt pavement. Asphalt pavement mixtures modified by crumb rubber (CR) and chemically modified crumb rubber (CMCR) with three notch lengths were compared to a control using the critical strain energy release rate, J_C. Peak values for specimens with 1 in (25.4 mm) notches averaged 259 lb (1.15 kN), 1.25 in notch specimens averaged 187 lbs (0.83 kN), and 1.5 in notch specimens averaged 135 lb (0.6 kN). The authors showed that the CMCR mix had the highest value for J_C and hence the most resistance to cracking and the control was least resistant to cracking. And by comparing the values calculated for the three mixes to those calculated in other studies, the authors showed that J_C produces consistent results and could be utilized for future study.

Hofman et al (2003) conducted static and cyclic experiments on SCB samples. Their paper described the difficulty of measuring the crack length by means of four methods: crack foil, crack opening displacement (COD), mortar displacement, and optical capture by digital camera. The study concluded that measuring crack length for the determination of crack length increase per cycle still proves to be inaccurate and challenging, although the digital camera method excelled by capturing the bifurcating structure of the cracks. A method for calculating K_{IC} was provided with reference to another study. The static load tests confirmed the effects of mixture properties on cracking using K_{IC}. The repeatability and reproducibility of the results of the static SC(B) test were low compared to other mechanical tests for asphalt mixtures.

Wu et al. (2005) used the J-integral to characterize thirteen different Superpave mixtures with four different binder types (PG 70–22, AC–30, PAC–40, and PG 76–22) at four different compaction levels (N_{design} = 75, 97, 109, and 125), and three different notch lengths [1 in (25.4 mm), 1.25 in (31.8 mm), and 1.5 in (38 mm)]. A statistical analysis was performed on the following test results: peak load, vertical displacement, and strain energy to failure. The PAC–40 mixture had the largest Average peak load value [364 lb (1.62 kN)] followed by each binder type in descending order PG 76–22 [344 lb (1.53 kN)], AC–30 [330 lb (1.47 kN)], and PG 70–22 [252 lb (1.12 kN)]. In addition, the calculation and analysis of the J-integral using samples of variable notch length was stressed. The method of obtaining J_C in the SCB sample is documented and test data. The authors determined that J_C is superior in consistently characterizing mix types with varying binder types and compaction levels in comparison to fundamental test results such as peak load, vertical displacement, strain energy to failure.

Wagoner and his colleagues (2005a) deemed the SE(B) geometry the most promising and conducted static tests at low temperature to investigate cracking in asphalt concrete. Crack mouth opening displacement (CMOD) and load were captured for input to a numerical model, the cohesive zone model (CZM). Wire crack detection gauges were used to detect crack initiation at the notch tip. Crack initiation was detected slightly after the occurrence of ultimate load. The tests showed that lower temperature produced lower fracture energy for all mixes, and smaller nominal maximum aggregate size (NMAS) produced higher fracture energies.

The same year, Wagoner and his colleagues (2005b) published an investigation of the DC(T) specimen for the analysis of cracking in asphalt concrete. Concerns about the size effect present in the SC(B) specimen and the ability to test specimen obtained by coring lead to the choice of the DC(T) geometry as a candidate for fracture testing in asphalt concrete. Load and CMOD data were captured in order to calculate the fracture energy of each specimen. Testing was conducted on samples of varying temperature [32°F(0°C), 14°F(-10°C), -4°F(-20°C)] and four different mix types ranging from high, modified binder content to low, unmodified binder content. The tests showed increasing fracture energy with increasing temperature. The reliability of the tests was with an acceptable range, but indicated that more research should be conducted on the size affects of fracture parameters.

The above summaries describe the recent advancements in the study of laboratory cracking in asphalt concrete. It can be said that a definitive method of characterizing a asphalt mixture's susceptibility to cracking has yet to be defined. The following chapter describes the laboratory testing involved in this study.

The studies summarized in this literature review describe past work involving strength testing and fracture testing of asphalt concrete. Generally, these studies are focused on evaluating the effects of additives in asphalt concrete or on the development of a standard test to determine the fracture properties of asphalt concrete. Together, these types of studies comprise the state of the art in laboratory fracture testing of asphalt concrete.

CHAPTER 3

Laboratory Testing

3.1 Introduction

This chapter presents the details of specimen preparation and testing. Crack Opening Displacements (COD) and loads are recorded in real time using four linear variable displacement transducers. Three plant manufactured mixes were collected from a local company. The specimens were compacted and then sliced to the correct testing geometry. Specimens are subjected to a strain controlled compressive load in three point bending. Load versus displacement data for each specimen is captured in real time using a load cell, LVDTs, and a data acquisition system powered by a Labview program.

Asphalt concrete is a mixture of asphalt coated aggregate particles. The complex structure of asphalt concrete is simplified for modeling purposes. The asphalt mix can be thought of as a sum of two components: the larger sized coated aggregate and a smaller sized coated aggregate. In this study, the coated materials that pass the #4 sieve is called matrix.

The possible modes of failure in the notched asphalt specimen are shear failure due to compression in the matrix, tensile failure in the matrix, shear failure at the aggregate–matrix interface, and tensile failure at the aggregate–matrix interface. Aggregate has high tensile, compressive, and shear strengths compared to mastic or aggregate-mastic interface. Laboratory tests are designed to capture the load versus displacement relationships to the point of failure for each of these failure mechanisms.

Additionally, tests are conducted on both dry and wet samples to investigate the effects of sample wetting. Sample preparation, procedure, and results for each test are described below:

3.2 Materials

Three Superpave mixes were collected from a local plant in cooperation with the New Mexico Department of Transportation. Mixes were selected to cover both fine and coarse mixes used in New Mexico. Figure 3.1 is a aggregate distribution chart for the three mixes used in this study. Maximum density lines are plotted for both maximum aggregate sizes present. It is shown in Figure 3.1 that mix SP-C has a smaller maximum aggregate size than mixes SP-B and SP-III. Mix gradations that plot above the maximum density line tend to be fine mixes, while gradations below the maximum density line tend to be coarse mixes. The maximum density lines for maximum aggregate sizes of 3/4 in and 1 in are plotted in Figure 3.1. SP–C has a maximum aggregate size of 3/4 in where as mixes SP-B and SP-III have a maximum aggregate size of 1 in. Mixes that plot above the maximum density line are generally fine mixes while mixes that plot below the maximum density line are generally coarse mixes. Superpave mixes SP-B and SP-C plot above their respective maximum density lines and mix SP-III plots below its respective density line. Therefore, mix SP-III is a coarse mix and mixes SP-B and SP-C are fine mixes. Of the fine mixes, SP-B is coarser than SP-C.

To prepare matrix samples for testing, loose mix material is heated at 160 degrees for just enough time so that the mix material is separable into its constitutive coated aggregate

sizes. Once heated, the mix is agitated on a flat surface by hand until the mix cools below a temperature at which the binder is sufficiently liquid enough to result in binding of the aggregate. The mix is then shaken over a customary U.S. sieve of size designation #4 (0.187 in). All of the loose mix material passing the #4 sieve cumulatively is defined as the matrix of the asphalt concrete mix.

3.3 Semi-Circular Samples

Sample Preparation

Each of the mixes is compacted into 6 in (15.25 cm). diameter cylinders by a Superpave gyratory compactor using a 87.02 psi (600 kPa) vertical pressure (AASHTO T 312). Sample height is kept to about 5.0 in (12.7 cm). Next, using a water-cooled laboratory saw, two one-inch thick discs are sliced from the center of each cylinder in an attempt to acquire samples with uniform air voids. Finally, the discs are halved and notched in the center of the flat edge with 3/8 in (9.525 mm) deep slits using a laboratory saw of 1/8 in (3.175 mm) blade thickness. Figures 3.2(a)-(c) show the compacted asphalt concrete cylinder, sliced discs, and notched samples, respectively.

This study aims to characterize the cracking in asphalt concrete of differing air void ratio and moisture condition. Therefore, six samples for each mix were prepared with varying void ratios and moisture condition. Two samples are prepared at a low air void ratio (≤ 4% air voids), two samples at a medium air void ratio (4% ≤ air voids ≤ 7%) and two samples at a high air void ratio (≥ 7% air voids) (ASTM D-2726 1996). One sample for

each void ratio range is subjected to moisture conditioning by standard method AASHTO T-283 and one sample is kept dry and undamaged by moisture (AASHTO T 283 2002).

Notch Tip Location

Figure 3.3 depicts the three notch tip locations. The classification of the notch type involves visual inspection to determine the approximate percentage area of the notch's tip through the thickness of the sample that is embedded in aggregate, mastic, or interface. Depending on the maximum notch tip percentage, a notch type is chosen. For example, if a notch tip is embedded in aggregate through 60% of the sample's thickness, interface 30%, and mastic 10% the notch is considered an aggregate notch tip.

Sample Testing

The loading configuration for the notched sample is shown in Figure 3.4. It can be seen that four LVDTs are mounted 0.75 in (19.05 mm) above one another beginning at the notch tip in order to measure horizontal displacement at different locations on the sample. Because the horizontal displacement tended to diminish toward the upper portion of the sample the LVDTs are ordered in decreasing range from the bottom edge of the sample to the top loading point. The ranges of the LVDTs are 0.25 in (6.35 mm), 0.1 in. (2.54 mm), 0.1 in., and 0.005 in. (0.127 mm).

The sample is loaded vertically at a constant strain rate of 0.01 in/min (0.254 mm/min). This loading rate was determined based on trials at different rates. It was found that a rate of 0.01 in/min is optimal in inhibiting cracking at the supports while inducing

cracking at the notch tip. The LVDTs are mounted using epoxy and connected to the Labview Data Acquisition (DAQ) system. The LVDTs are mounted around a narrow region above the notch point so as to detect only the strain and crack opening displacement directly associated with crack initiation and propagation. The wet samples are allowed to surface dry for approximately five minutes to promote sufficient adhesion to the LVDT mounting blocks. Samples are loaded until the sample develops a visible crack or fracture.

Reliability

Reliability of sample preparation and testing procedure was evaluated by preparing six specimens of the same mix type, air void content, and notch type. Three of the samples were soaked in water for 24 hours prior to testing and three were kept dry. Table 3.1 presents data from the testing of these specimens. The table includes: ultimate load, COD at ultimate load, crack initiation potential, fracture load, slope of the crack propagation curve, and initial crack velocity. For each parameter the standard deviation and coefficient of variation is calculated. It can be seen in the table that the coefficient of variation is less that 15% for all parameters other than the crack initiation potential. This indicates that sample preparation is reliable enough to produce consistent results for similar specimen types.

3.4 Matrix Testing Samples

3.4.1 Matrix Tension Test

Sample Preparation

The cylindrical samples used for the matrix tension test are molded inside Harvard miniature molds. These samples were prepared to a target void ratio of 4.0 ± 0.5%. The void ratio is calculated by the mass of matrix material needed to fill the mold volume of 4.17 in^3 (68.4 cm^3) using a maximum specific gravity of 38.673 g/in^3 (2.360 g/cm^3) and 4.0 ± 0.5% air voids. The amount of mix needed to meet the void ratio requirement is 155.0 g.

The matrix material is heated in an oven at 307°F (153°C) for one hour and then compacted in the cylindrical mold in three lifts. The lift surface faces are scored in order to assure proper bonding of the lifts so that weak lift to lift interfaces are eliminated. Immediately after compaction the sample is extruded from the mold and allowed to cool to room temperature. Figure 3.5 shows the sample preparation materials and some compacted matrix material. When cool, the samples are sliced using a lab saw at both ends to 2.75 in (6.985 cm) in length so as to eliminate excessive voids at the ends of the sample. The sample is assured to be twice the diameter of the sample. For wet conditioning, samples are soaked for 48-hours under water at room temperature and pressure.

Testing Configuration

Figure 3.6 shows the testing configuration for the matrix tension test. The sliced ends of the cylindrical sample are fixed with a high strength epoxy. An interface plate is used to ensure that constant stress is applied over the sample end area. Epoxy is applied to the bottom interface plate and sample is placed on top so that the sample sets evenly on the surface. After the bottom interface has strengthened, the sample is fixed to the Universal Testing Machine (UTM) at the bottom with a pin and epoxy is placed on the top sample surface. The crosshead is then raised so that the top post comes into contact with the epoxy in a load free configuration. This procedure was established after many attempts at preventing failure between the epoxy and the interface plate.

3.4.2 Matrix Compression Test

Sample Preparation

The cylindrical samples for the matrix compression test are the same as the samples used in the matrix tension test. So the procedure for preparing samples for the compression test is exactly the same as the procedure to preparing samples for the tension test. Two samples were prepared, one was kept dry and the other was wetted by soaking in water for 48-hours.

Testing Configuration

The testing configuration for the compression test is very similar to the tension test. Figure 3.6 shows the sample and machine ready for testing. When the sample was in

compression there was no need to use epoxy to fix the sample ends in the vertical direction.

3.4.3 Aggregate Pull-off Test

Sample Preparation

The wet and dry samples are compacted to a target void ratio of 4 ± 0.5%. Each sample is compacted in a moisture tin. The weight of the matrix material is calculated to fill a volume equal to 5.53 in^3 (16.39 cm^3). The mass of matrix material needed to meet the void ratio requirement is found to be 205.34 g.

The matrix material is weighed and placed in an oven to heat for 1 hour at 307 °F (153 °C). A coated aggregate is sliced parallel to one of the fractured faces of the aggregate and then placed in the oven with the mix to heat to the compaction temperature.

The matrix material is compacted in three lifts by hand using a metal tamp. The lifts surfaces are scored after tamping to reduce the possibility of a weak lift to lift interface. Prior to the final tamping of the top most lift, the fractured face of an asphalt coated aggregate is pressed against the matrix so as to ensure contact between the matrix material and the aggregate face. The wet samples are soaked in water at room temperature at atmospheric pressure for 48-hours.

Testing Configuration

The sample is tested in tension above the crosshead using a UTM. Figure 3.7 shows the physical test setup for the aggregate pull-off test. The bottom of the sample is secured with a high strength epoxy to a steel plate and the plate is set on top of another moisture tin which acts as a spacer that places the sample into the operating range of the crosshead. The steel plate is fixed in the vertical direction on both sides of the sample to the crosshead using a system of steel bars above and below the crosshead that are linked with all-thread, nuts, and washers. At the top of the sample, a metal post with a flat surface facing downward is pinned to a joint that designed to eliminate unintentional moments on the sample that are introduced during loading. It is important to reduce the possibility of off-axis loading so that the UTM imposes only a tensile load on the aggregate/matrix interface. An unintentional moment imposed on the sample will result in a non-uniform stress at the aggregate/matrix interface. To assure that the load at the interface is primarily tensile the epoxy is placed on the aggregate surface and then the crosshead is raised to the post were the epoxy cures in an unloaded position. The epoxy is allowed to cure for 24-hours before the sample is tested to ensure full strength at the aggregate/machine interface. The sample is then load in tension at a rate of 0.05 in/min. Load and displacement data are collected in real time using the IEEE interface that is electronically tethering the computer based data acquisition system to the UTM.

3.4.4 Direct Shear Test

In this study the shear strength of the aggregate/matrix interface was tested in shear. The test provides a load versus displacement curve that can be used to determine the reaction

of an aggregate element to the shear force caused by a matrix element and vise versa. When the maximum load in the shear load versus displacement curve is exceeded slippage occurs in the model. The area of the interface is determined in order to normalize the load versus displacement curves for the dry and wet samples.

Sample Preparation

Samples were prepared to a target void ratio of 4.0 ± 0.5%. This requirement was met by calculating the amount of matrix material necessary to fill the bottom half of the direct shear box using a specific gravity equal to 38.673 g/in^3 (2.360 g/cm^3) leaving room for 4 ± 0.5% air voids. The mass of matrix material needed to fulfill the void ratio requirement is 117 g.

The required mass of matrix material and an aggregate are placed in an oven and heated for one hour at 307 °F (153 °C). The hot matrix material is then compacted in two lifts into the bottom half of the shear box. Just before the final compaction of the top layer a coated, fractured face of the hot aggregate is pressed onto the surface of the top lift and the compaction to the required volume is then completed to ensure proper contact between the aggregate and the matrix. The aggregate volume is firmly contacting the matrix before the sample is left to cool. One sample is left in a dry condition and the other is soaked in room temperature water at atmospheric pressure for 48-hours.

Test Configuration

The top of the shear box is placed on the bottom of the shear box and the apparatus is placed into the direct shear machine. The set screws in the shear box are removed and the height of the top of the shear box is raised so that no matrix material impedes the shearing of the aggregate. The bottom of the shear box is then advanced in order to bring the top of the shear box into contact with the aggregate. Figure 3.8 shows the configuration of the apparatus before the test.

CHAPTER 4

Analysis of Cracking Parameters

4.1 Introduction

Cracking in asphalt concrete is a two stage process involving the initiation of a crack followed by propagation. LEFM and EPFM theory has lead to parameters such as the critical stress intensity factor, K_{IC}, and the fracture energy, J_{IC}, respectively. These parameters quantify the susceptibility of a specimen to cracking, but are cumbersome to obtain in a laboratory setting. Therefore, cracking parameters that are derived directly from load and displacement data are advantageous when laboratory evaluation of asphalt concrete is necessary.

This chapter describes the analysis of six cracking parameters determined from laboratory testing of the SCB specimens. Table 1 shows Test Matrix A, a total of 24 samples with different properties were tested for the evaluation in this chapter. Half of the samples are compacted to 7% void ratio and the other half to 4% void ratio. Half of the samples are soaked in water for 24 hrs prior to testing to induce moisture damage on the sample. Focus is given to the notch tip location in order to emphasize variations in crack initiation. Two replicates of each sample type are tested.

The parameters used to characterize crack initiation are the ultimate load (P_{ult}), the cracking potential (U_{ult}), and the LVDT 4 crack opening displacement at ultimate load (COD_{ult}). The cracking potential is defined as the area under the load versus COD curve up to the crack initiation point. Three parameters are used to characterize the crack

propagation phase. These parameters are the fracture load (P_f), which is the load at fracture, the slope of the crack propagation path (θ), which is the change in load for a COD value of 0.035 in. past COD_{ult}, and the crack velocity (v), which is defined in a later section of this paper. In summary, three parameters (P_{ult}, COD_{ult}, and U_{ult}) are used to characterize crack initiation and three parameters (P_f, θ, and v) are used to characterize crack propagation while varying notch type, void ratio, and moisture condition.

4.2 Laboratory Parameters

Figure 4.1 is the load versus horizontal displacement data for four LVDTs for a sample of mix SP–B. The load versus horizontal displacement curve in Figure 4.1 is divided into two portions: the crack initiation phase and the crack propagation phase. The portion of the loading curve beginning at the onset of loading up to the crack initiation load is the crack initiation phase of the cracking process. In this phase micro cracks and micro voids are formed without reduction in loading. The crack becomes visible at the crack initiation load (P_{int}), which is defined as the crack initiation point. This value is determined by laboratory observation. Any increase in the horizontal displacement after crack initiation is considered actual crack width, or crack opening displacement. The sample continues to sustain increasing load as the crack propagates through the sample. The sample attains ultimate load (P_{ult}) at maximum point of the load versus displacement curve. After which, the load starts to decrease as the COD increases. A finite crack is visible in all samples when LVDT 4 measures a COD value of 0.035 in. after the COD value at ultimate load. In this study fracture is defined when the COD value reaches 0.035 in past the COD at ultimate load. From laboratory observation, the authors

discovered that in some of the samples, if testing continued 0.035 in beyond COD_{ult} several cracks occur in the sample. This makes it extremely difficult to capture the crack width, which is the main objective of this study.

While P_{int} can be used as a measure of crack initiation and P_{ult} indicates the overall strength of the sample, the difference between the ultimate load and the crack initiation load (P_{ult} - P_{int}) is used to characterize a sample's resistance to failure due to cracking. For example, a sample that can withstand 50 lb additional load after crack initiation as opposed to 20 lb additional load has a higher strength in the presence of cracking.

Two parameters are used to characterize propagation: the crack velocity (v) and the slope of the crack propagation curve (θ). The crack velocity is defined in a later section of this document. The slope of the crack propagation curve (θ), is the change in load (dP) for a COD value of 0.035 in. past the COD at ultimate load.

4.3 Crack Path in Asphalt Concrete

Figure 4.2 shows a typical crack propagation path as observed in the laboratory. Crack propagation is shown in Figure 4.2 by use of three photos taken during testing of a mix SP-B sample. In Figure 4.2(a), the crack initiates at the notch tip. The chalk around the notch tip helps to make this crack initiation more visible so as to accurately note the time and load of crack initiation. Figure 4.2(b) shows the common occurrence of crack propagation along aggregate-mastic interfaces. In addition, Figure 4.2(b) shows that one aggregate-mastic interface becomes less preferable for crack propagation, the crack path

will transfer quickly to another interface. Abrupt transfer of a crack between aggregate-mastic interfaces demonstrates the crack's preference for propagation along an interface. In Figure 4.2(c), the crack is shown to propagate in a staggered path due to the lack of a conveniently located interface. This crack wandering suggests that cracking in the mastic occurs without a defined pathway.

4.4 Determination of Crack Velocity

Crack velocity is calculated from the COD and time. Crack velocity is defined as the distance traveled by the crack (Δl) divided by the time elapsed. That is:

$$\nu = \frac{\Delta l}{\Delta t} \tag{1}$$

$$\begin{aligned} \textit{where: } \nu &= \textit{velocity} \\ \Delta l &= \textit{crack length} \\ \Delta t &= \textit{time elapsed} \end{aligned}$$

Figure 4.3 shows a schematic of a crack (same width) appearance at two difference locations. At time, $t=t_1$ the crack initiates ($COD=COD_{ult}$) at the crack tip or LVDT 4. From the data acquired, the time ($t=t_2$) can recorded when the same width (COD_{ult}) appears at LVDT 3 location. As a result, $\Delta t = t_2 - t_1$ and distance travelled by the crack, $\Delta l = 0.75$ (distance between the LVDT 4 and LVDT 3). Velocity can be calculated by using these values in Eq. 1; however, this is an average velocity in the region between LVDT 4 and LVDT 3. For a continuous velocity profile, time series of data collected by LVDTs are used to find the distance travelled by the crack of same width (i.e. COD_{ult}). The following paragraph explains how the time series of LVDT data are used to determine the distance travelled by the a crack.

The four LVDTs implemented in this study detect the presence of the crack by reading out a value for horizontal displacement equal to COD_{ult}, which is the the crack initiation width for a given sample. When this value is detected in subsequent LVDTs as the crack propagates, the distance travelled by the crack can be determined with reference to time or load. For example, when COD_{ult} is measured by LVDT 3, the crack is considered to have traveled 0.75 in from LVDT 4 to LVDT 3. Based on this principle, it is possible to interpolate the location of the crack initiation point, or the length of the crack, at any given time. This is accomplished by use of a chart shown in Figure 4.4.

In Figure 4.4, half of the horizontal displacement is plotted as a function of distance from the notch tip. Each line is plotted using four data points, one from each LVDT at a given time. In order to interpolate the crack length a horizontal line is drawn through the COD value (0.015 in) at LVDT 4 corresponding to crack initiation, COD_{ult}. The intersection of this horizontal line with any one of the other lines is considered as the location of the crack tip at that time interval. The distance of such intersection points from the origin are noted as the distance from the notch tip to the crack tip, or the distance traveled by the crack. The vertical dotted lines are plotted in Figure 4.4 show the increasing distance traveled by the crack tip at equal time intervals. Crack velocity is calculated using this distance at different time intervals. It is clear as the crack travels from the notch tip to the top of the sample that the velocity of the crack decreases.

Figure 4.4 can be exploited in order to understand three different regions along the crack propagation path: the compression region, the tensile deformation region, and the crack widening region. The compression region in the sample denotes locations where the LVDT has recorded negative COD values. The tensile deformation region in the sample is located where no crack is present (below the horizontal line where COD = 0.015 in = COD_{ult}), but positive values are recorded by the LVDTs. The crack widening region is above the horizontal line passing through the COD at the crack initiation point. From Figure 4.4, it is evident that there is not a linear relationship between crack widening and crack growth.

In the following section, the effect of varying mix type, air void ratio, and moisture condition are evaluated using the defined parameters above.

4.5 Evaluation of Crack Initiation Parameters

4.5.1 Ultimate Load, P_{ult}

Figure 4.5 is a bar chart showing the average and actual ultimate loads for three notch types at 4% and 7% void ratio under dry and wet moisture conditions. The effects of notch type, sample conditioning and void ratio on ultimate load are discussed below.

Effect of Notch Type on P_{ult}

From Figure 4.5, it can be seen that samples with an aggregate notch type have higher ultimate loads than the samples with interface or mastic notch types. This is expected because aggregate is usually stronger than mastic or binder in an asphalt concrete. It is

evident from both Figures 4.5(a) and (b) that the ultimate load does not differ significantly between samples having a mastic notch type and samples having an interface notch type. Ultimate load indicates a sample's resistance to crack initiation. Therefore, mastic and interface notch type samples exhibit similar resistance to cracking.

Effect of Moisture Condition on P_{ult}

Figure 4.5 indicates that cracks initiate at higher ultimate loads in wet samples than those in the dry samples. This may be explained by damage that is observed at the supports during the loading process. It is known that moisture causes damage (adhesive and cohesive damage) in asphalt concrete**.** The damaged or soft samples more readily deform at the supports rather than show cracks at the notch tip. Crack opening at the notch tip requires bending instead of deformation at the supports. On the other hand, stiff or hard samples will not show damage at the support, rather it will more likely crack at the notch tip due to bending. Therefore, when the samples in this study are damaged by moisture, the deformation at the supports due to loading may decrease the amount of bending required for crack initiation resulting in larger ultimate loads.

Effect of Void Ratio on P_{ult}

Figure 4.5(a) shows the ultimate load for samples with 4% void ratio while Figure 12(b) shows the ultimate load for samples with 7% void ratio. Overall, it can be seen that the ultimate load does not vary consistently with a change in void ratio. This is likely because crack initiation occurs at the notch tip, which is only a point compared to the entire area of the sample over which the air voids are distributed. This is more true when

comparing mastic and interface notch type samples in Figures 4.5(a) and (b). However, for the case of wet aggregate notch type, samples with 4% air voids have shown higher ultimate loads at crack initiation than samples with 7% air voids.

4.5.2 Crack Opening Displacement at Ultimate Load, COD_{ult}

Figures 4.6(a) and (b) show the average and actual crack opening displacement of samples with 4% and 7% air voids. The larger the COD, the more lateral displacement near the notch tip before crack initiation point.

Effect of Notch Type on COD_{ult}

From Figure 4.6(a) and (b), there is no clear trend in COD value due to aggregate, mastic, and interface notch types. The COD results from lateral displacement due to the opening of micro voids and micro cracks due to tensile stress and sagging of the sample due to bending. The COD_{ult} value reflects the displacement of the entire matrix of material between the LVDT mounting blocks rather than just the material at the notch tip. Therefore, the notch type has very little effect on COD_{ult}.

Effect of Moisture Condition on COD_{ult}

When comparing wet versus dry samples for 4% air voids (Figure 4.6(a)), the wet mastic and interface samples show higher COD values than the dry samples. This result indicates that the wet samples will deform more laterally compared to the dry samples. In dense samples (4% air voids), deformation is due to shear flow, therefore the material displaced laterally in order to maintain volume continuity. In contrast, when comparing

wet versus dry samples for 7% air voids (Figure 4.6(b)) the wet mastic and interface samples have smaller COD values than the dry samples. The vertical deformation in 7% air voids samples occurs due to compaction. Furthermore, soft, wet samples compact more than hard, dry samples, thereby resulting in a reduction of lateral displacement in wet samples. It is difficult to explain the difference in COD values between wet and dry samples with aggregate notch type using this COD parameter.

Effect of Void Ratio on COD_{ult}

The effect of void ratio on COD_{ult} is explained in the previous paragraph. The main difference in COD between 4% and 7% air void samples is due to the deformation mechanisms, which are shear flow and compaction for the 4% and 7% air voids samples, respectively.

4.5.3 Cracking Potential, U_{ult}

Figures 4.7(a) and (b) show the average and actual cracking potentials of asphalt concrete samples at 4% and 7% air voids. Cracking potential is defined as the strain energy stored in the sample during the crack initiation phase. Samples store energy through micro-void opening and micro–fiber straining under the applied load.

Effect of Notch Type on U_{ult}

Figure 4.7(a) shows that the samples with an aggregate notch type have higher cracking potential values than the samples with mastic and interface notch types. Figure 4.7(b) shows that the wet sample with an aggregate notch type has a higher cracking potential

compared to the wet samples with mastic and interface notch types. This, however, is not true for the dry samples. Therefore, there is no clear trend of the effect of notch type on cracking potential.

Effect of Moisture on U_{ult}

It is clear in Figures 4.7(a) and (b) that the wet samples have higher values for cracking potential than the dry samples. This illustrates that wet samples store more energy than the dry samples before crack initiation. Also, it can be noted that in the case of mastic and interface samples the increase in cracking potential is significant at 4% air voids. From this study, it is not possible to explain how the moisture conditioning has affected the ductility of the asphalt concrete. This will require an understanding of bonds at asphalt-water-aggregate interfaces, which occur at the molecular scale. Such an analysis is beyond the scope of this study.

Effect of Void Ratio on U_{ult}

From Figures 4.7(a) and (b) it can be seen that dry samples with 4% air voids have lower cracking potential compared to the dry samples with 7% air voids. Samples with 7% air voids are expected to have lower stiffness than the samples with 4% air voids. Also, Figures 4.7(a) clearly shows that samples at 4% void ratio have a consistent increase in cracking potential when wet. The increase due to wetting in 7% void ratio samples is largest for the sample with an aggregate notch type, while the increase in the mastic and interface notch type samples due to wetting is smaller. It appears that increasing the amount of air voids decreases the dry sample stiffness, and increasing air voids in wet

samples increases the stiffness. Therefore, no clear trend of how air voids affects cracking potential is evident from this study.

4.6 Evaluation of Crack Propagation Parameters

4.6.1 Fracture Load, P_f

Figures 4.8(a) and (b) show average and actual fracture loads for samples with 4% and 7% void ratios. As mentioned earlier, the fracture load is an indication of the sample's load carrying capacity at fracture. The following paragraphs discuss the effect of notch type, moisture condition, and void ratio on the fracture load.

Effect of Notch Type on P_f

Figures 4.8(a) and (b) indicate that the aggregate notch sample sustains the largest load at fracture. Samples with mastic and interface notch types exhibit similar fracture load. This is likely because samples with aggregate notch type have higher peak values at crack initiation compared to the samples with other notch types. This indicates that the notch location does have an effect on cracking

Effect of Moisture Condition on P_f

Overall, Figures 4.8(a) and (b) show that the wet samples have higher load at fracture than the dry samples. As shown previously, wet samples have higher ultimate load, which may result in higher fracture load.

Effect of Void Ratio on P_f

Overall, the values for fracture load are larger for the 4% void ratio samples than for the 7% void ratio samples. This is similar to what is seen in the case of ultimate load previously. Fracture load is probably is not a good parameter to distinguish sample's fracture behavior due to air voids.

4.6.2 Average Slope of the Crack Propagation Curve, θ.

The average slope of the crack propagation path is defined as the slope of the load versus COD curve after the ultimate (peak) value of the load. A higher value of the slope means there is more cracking in the sample, because the cracking is the primary mechanism for the decrease in magnitude of the applied load. Figures 4.9(a) and (b) show the average slope of the crack propagation curve for 4% and 7% void ratios, while figures 4.9(c) and (d) show the actual values for each tested specimen. The slope represents crack propagation during 0.035 in. of crack width increase at the notch tip beyond COD_{ult}.

Effect of Notch Type on θ

From Figures 4.9(a) and (b), overall the mastic and interface samples exhibit similar behavior in the slope of the crack propagation curve. Mastic and interface strengths originate mainly from binder cohesion, therefore a crack propagating through similar materials, which behave similarly. On the other hand, Figure 4.9(a) shows that the aggregate notch type sample has the lowest value for the slope, but Figure 4.9(b) shows that the aggregate notch type sample has the highest value for the slope. This difference can be explained using two cases of crack propagation in samples with aggregate notch

type observed in the laboratory. In one case, the crack propagates by splitting of the aggregate located at the notch tip. In the other case, the crack does not split the aggregate located at the notch tip, rather the crack initiates at the nearest interface along the notch surface.

Effect of Moisture on θ

The wet samples with aggregate notch type in 7% air voids samples don't indicate an increase in slope, moisture conditioning increases the magnitude of the slope overall. Therefore, wet samples tend to show higher load decrease (higher slope) during crack propagation than the dry samples. This is in contrast to the earlier finding that wet samples resist crack initiation more so than dry samples. During crack propagation, a crack has to separate bonds in the mastic or asphalt binder to open the crack. Moisture weakens the bonds in the asphalt-aggregate system and allows for easier crack propagation through the samples weakened by moisture than through the dry samples.

Effect of Void Ratio on θ

The wet samples at 7% air voids have higher magnitude in the slope compared to the slopes at 4% air voids. This trend can also be seen for the dry samples. This shows that once the crack has initiated, the crack propagation is dependent upon the void ratio of the samples. When a crack propagates, if the crack encounters a void no additional work is needed to continue crack propagation. On the other hand, if the crack encounters an aggregate particle or a mastic volume, additional work is necessary to separate the matrix resulting in a smaller value for the slope.

4.6.3 Crack Velocity, *v*.

Effect of Notch Type on *v*

Figures 4.10(a) and (b) show samples under dry and wet conditions with 4% void ratio while Figures 4.10(c) and (d) show samples under wet and conditions with 7% void ratio. At 7% air void all of the notch types show similar behavior, however at 4% air voids there is not clear trend in the peak velocity due to notch type.

Effect of Moisture Condition on *v*

Figures 4.10(a) and (b) show crack velocity for dry samples, whereas Figures 4.10(c) and (d) show crack velocity for wet samples. Clearly, there is no effect of wet/dry conditions on the peak velocity. On the other hand moisture conditioning has affected the peak velocities of samples with 4% air voids. The aggregate and interface notch type samples both exhibit an increase of peak velocity due to wetting, while the mastic peak velocity shows a decrease. The mastic notch sample shows the most drastic change due to wetting in 4% air voids. It is likely that the mastic has incurred the most damage.

Effect of Void Ratio on *v*

Figure 4.10 clearly shows that samples with 7% air voids have cracks with lower peak velocities compared to those in samples with 4% air voids. At lower air voids, materials being more continuous have lesser number of voids at which crack propagation is interrupted. Additionally, peak velocities drop sharply in samples with 4% air voids compared to samples with 7% air voids.

4.7 Observations

From this study, the following remarks can be made:

- Cracks tend to propagate along the interface of aggregate and the matrix.

Some observations related to P_{ult} when characterizing crack initiation:

- Aggregate notched samples show higher P_{ult} while mastic and interface notch types perform similarly.
- Moisture conditioning results in damage that leads to higher values for the ultimate load.
- Void ratio has apparently no effect on ultimate load.

Some observations related to COD_{ult} when characterizing crack initiation:

- Notch tip location has no effect on the COD_{ult}.
- Because of compaction at the supports, COD_{ult} is low in 7% air voids samples compared to COD_{ult} in 4% air voids samples.
- Moisture exacerbates the effects of void ratio on COD_{ult}.

Some observations related to U_{ult} when characterizing crack initiation:

- There is no clear trend of the effect of notch type on cracking potential.
- U_{ult} shows that wet samples are able to store more energy during the crack initiation process, hence less cracking.
- No clear trend of how air voids affects cracking potential is evident from this study.

Some observations related to P_f while characterizing crack propagation:

- The trend for fracture load is similar to that for crack initiation load.

- Wet samples exhibit a higher load at fracture than dry samples.
- The fracture load parameter didn't show any effects of void ratio.

Some observations related to θ while characterizing crack propagation:

- The value of the slopes of the crack propagation curve for interface- and mastic-tip samples are similar, while aggregate notch type sample has a slope dependent upon the crack path.
- Wet samples tend to show higher load decrease (higher slope) during crack propagation than the dry samples.
- The slope of the crack propagation curve shows that cracks propagate more easily in samples with high air voids.

Some observations related to v while characterizing crack propagation:

- There is no effect of notch type on peak velocity.
- Moisture had an effect on the peak velocities of dense samples, but none on more porous samples.
- Cracks propagate faster initially in dense samples than in porous samples.

4.8 Conclusions

In summary, P_{ult} performs best in characterizing crack initiation by distinguishing well between samples of varying notch type and moisture condition. None of the crack initiation parameters showed that crack initiation is affected by void ratio. Overall, these parameters show that cracks initiate more readily in the mastic or at an interface within the asphalt concrete sample. Also, because of damage at the supports, wet samples showed more resistance to crack initiation. Parameters v and θ work well in conjunction

to describe the affects of notch type, moisture condition, and void ratio on crack propagation. Notch type had no effect on crack propagation with the exception of varying crack path in the case of aggregate notch type samples, as revealed by θ. An increase in cracking potential due to moisture was evident with the use of θ. The contribution of void ratio in aiding the process of crack propagation was demonstrated by increased v in 7% air voids samples.

CHAPTER 5

Analysis of Cracking in Superpave Mixes

5.1 Introduction

Cracking in asphalt concrete aids in the introduction of water to a mix which can lead to stripping of the binder from the aggregate. Current standards for the approval of an asphalt concrete mix design do not include limitations on cracking in a mixture. A comparison of Superpave mixes of varying gradation by use of laboratory testing would help in establishing a standard for cracking resistance in asphalt concrete. Few studies have evaluated fracture in notched specimens of various mix type (Wagoner et al. 2005b, Wu et al. 2005, Zhang et al. 2001). In addition, none of these studies have implemented the use of crack width away from the notch tip in data analysis. Crack width, as demonstrated in chapter 4, can be useful in determining the crack velocity within specimens of varying mix type, thereby offering an estimation of a pavement structure's service life.

In this chapter, specimen properties are evaluated using cracking parameters used in Chapter 4. Table 5.1 shows Test Matrix B, the distribution for the 18 specimens evaluated. Specimen properties highlighted in this analysis include mix type, void ratio, and the moisture condition. The range of void ratio has been expanded to investigate possible trends in cracking, and the AASHTO T283 procedure has been applied to half of the samples to standardize and amplify the moisture damaged condition. Video was taken of the cracking process and it was discovered that crack initiation occurred at a load slightly less than the ultimate load. The parameter P_{int} is introduced in order to

investigate crack initiation and the subsequent loading portion until ultimate load.

The parameter P_{int} is used as a measure of crack initiation and P_{ult} indicates the overall strength of the sample. The difference between the ultimate load and the crack initiation load (P_{ult} - P_{int}) is used to characterize a sample's resistance to failure to cracking. For example, a sample that can withstand 50 lbf additional load after crack initiation as opposed to 20 lbf additional load has a higher strength in the presence of cracking.

Two parameters are used to characterize propagation: the crack velocity (v) and the slope of the crack propagation curve (θ). In summary, one parameter (P_{int}) is used to characterize crack initiation, one parameter (P_{ult}) is used to characterize a sample's strength, and two parameters (θ and v) are used to characterize crack propagation while varying mix type, void ratio, and moisture condition.

5.2 Effect of Air Voids on P_{ult}, P_{int}, and v.

Figures 5.1(a) and 5.1(b) are scatter plots of the ultimate load (P_{ult}) and the crack initiation load (P_{int}) versus air voids for each sample tested in this study. A second order trend line is fit to the data in each plot. The equation for the trend line and the coefficient of variation is displayed on each plot. Similar plots can be made for the only the wet and dry samples respectively for the ultimate load and the crack initiation load. The equations for the trend lines and the R^2 values for these plots are listed in Table 5.2. The coefficient of variation (R^2), is significantly less than unity for each plot, although the R^2 for the wet samples only is near 0.5 for both P_{ult} *and* P_{ult}. Even though 0.5 is indicative that there is no trend, the consistently larger R^2 value for wet samples suggests that air

void ratio is more influential on the ultimate load and crack initiation load on wet samples than on dry samples.

Figure 5.2(a) shows the crack velocity versus the crack length in mix SP-B for three dry samples of varying void ratio and three wet samples of varying void ratio. It can be seen from the plot in that the samples of low and medium air void ratios show similar trends in crack velocity. The velocity starts highest at an initial value of about 3.25 in/min for the wet samples and about 5.25 in/min for the dry samples, and then decreases at similar slope until the end of the test. The samples with the highest void ratio exhibit higher initial crack velocity. The crack velocity in the high air voids samples appears to be most variable. It is possible that the increased amount of air voids in a sample leads to an increase in crack velocity by providing a crack pathway that requires less actual fracture of material.

It can be seen clearly in both Figures 5.2(a) and 5.2(b) that wet samples generally exhibit slower cracks. The moisture damage process softens a sample, creating more ductility that allows for greater amounts of bending before fracture.

5.3 Effect of Moisture on COD_{ult}, P_{ult}, P_{int}, and v

Figure 5.3 is a bar chart that shows the average crack opening displacement at ultimate load for all dry and wet samples of each mix type evaluated in this study. The range of the samples tested is shown with the error bars. The COD at ultimate load (COD_{ult}) is an indication of the amount of cracking necessary to induce failure in a sample. Figure 5.3

indicates that, in general, wet samples experience higher COD at ultimate load than dry samples. The average COD for the dry samples of all mix types is 0.021 in and the average COD for the wet samples of all mix types is 0.035 in. So, the moisture damage process facilitates the widening of cracks up to the point of ultimate load.

Figure 5.3 also shows that the highest values for COD_{ult} occur in mix SP-B while the lowest values occur for mix SP-III. Mix SP-B is a fine mix with a softer binder than the coarse mix SP-III. So, greater amounts of displacement should be expected in mix SP-B than mix SP-III. Mix SP-B contains a larger percentage of coarse aggregate than mix SP–C. The interface existing between coarse aggregate and mastic material is susceptible to damage and could allow for increased COD when compared to a sample with less coarse aggregate.

Figures 5.4(a) and 5.4(b) show the average ultimate load and average crack initiation load for wet and dry samples of each mix type. The error bars show the range of the samples tested. Figure 5.4(a) shows that the crack initiation load for dry samples in mixes SP-B and SP-C, while the crack initiation load in mix SP–III is higher for wet samples. This trend indicates that dry samples will take more load before crack initiation. This is expected since moisture is known to damage asphalt concrete. From Figure 5.4(b), the ultimate load for the wet samples is higher than or comparable to the ultimate load for dry samples. The average of the ultimate load for the wet samples is 302 lb, while the ultimate load for the dry samples is 282 lb. The moisture damage in asphalt concrete results in increased ductility. The ductility in the sample allows for higher levels of

strain. When the sample is strained the sample hardens as the air voids close. This effect is known as strain hardening.

Table 5.2 has a list of values for the difference between the ultimate load and the crack initiation load ($P_{ult} - P_{int}$). It can be seen from these load difference values that the values for wet samples are consistently higher than those for the dry samples. This trend indicates that after cracks have initiated in asphalt concrete, wet samples will withstand failure better than dry samples. This could be because wet samples are less brittle than dry samples.

5.4 Effect of Gradation on P_{int}, P_{ult}, v, and θ

Figures 5.4(a) and 5.4(b) show the average P_{int} and P_{ult} for wet and dry samples of each mix type with the range of samples tested denoted by error bars. For the average crack initiation load, it can be seen in Figure 5.4(a) that mix SP-III generally has the highest average crack initiation load while mixes SP-B and SP-C. Distinct differences between mix SP-III from mixes SP-B and SP-C are the stiffer binder contained in mix SP–III and the high percentage of coarse aggregate. Any of these two mix characteristics could be contributing to the observed trend.

Consider the average ultimate load for each mix type in figure 5.4(b). There is a general trend of increasing ultimate load and crack initiation load with SP-B being the lowest in load, and SP–III being the highest. This is explainable because mix SP-III is a coarse mix that is expected to withstand larger loads. Of the two finer mixes, SP-B and SP-C,

SP-B contains a higher percentage of coarse aggregate and therefore more interface along which a crack can continuously propagate.

Figure 5.2(a) shows the crack velocity for wet and dry samples of the three different mixes tested in this study. The crack velocity reveals no clear trend between aggregate gradation and cracking. One might expect that crack velocity be highest in coarser samples due to interface cracking.

Figure 5.5 shows the average slope of the crack propagation curve for each mix type. Mix SP-III has the largest slope of the three mixes and mix SP-B has the smallest slope. The slope of the crack propagation curve (θ) is a measure of the sample's resilience to cracking damage as the crack width increases. In that respect, the coarse mix has the least resistance to cracking damage. Preferred cracking along aggregate-mastic interfaces may indicate that the bond along the interface is weaker than that inside the mastic or aggregate. The large load decrease observed in mix SP-III can then be explained by realizing that mix SP-III is a coarse mix with large continuous interfaces along which cracks can propagate. These quasi-continuous crack path–ways facilitate extensive crack propagation and therefore high structural damage that leads to a decrease in load carrying capacity.

One might suspect that if coarse aggregate present in a mix leads to a large load decrease then mix SP-B should exhibit a larger load decrease than mix SP-C. The average value of load decrease for mix SP-C is somewhat misleading because one value is extremely

high, while the remaining values are generally less than 20 lb. If the outlying value for SP-C is overlooked, the average load decrease decreases to 34 lb. This hierarchy of load decrease well supports the interface cracking hypothesis.

5.5 Conclusions

In this study, different semi-circular notched asphalt concrete samples are subjected to continuously increasing static load. The resulting crack path and crack width are captured using LVDTs as a function of time and distance from the notch. Based on the analysis of laboratory data the following conclusions are made:

- Specimens with greater air voids showed faster cracks than specimens with lesser air voids.

- Cracks are wider at ultimate load in wet samples than in dry samples. Also, cracks propagate more slowly in wet samples. In addition, wet samples tend to resist failure after crack initiation better than dry samples as shown by higher P_{ult} and $P_{ult} - P_{int}$ values.

- The coarse mix in this study failed at higher loads than the fine mixes. Mixes with more coarse aggregate allow for continuous crack propagation along aggregate-mastic interfaces, leading to steeper unloading curves after the ultimate load. All three mixes showed similar crack velocities.

Chapter 6

Evaluation of Matrix Cracking

6.1 Introduction

Crack path may play an integral part in the cracking resistance of asphalt concrete as a crack will initiate within the weakest phase and then propagate along the path of least resistance. Evaluation of bond strength at the interface between aggregate and mastic and within the matrix of material aggregate passing the #4 sieve and binder can lead to insights on the nature of cracking in asphalt concrete. Identifying the weak points within an asphalt concrete can aid engineers in the design of asphalt concrete that is more resistant to cracking.

This chapter describes testing the matrix material and the interface between the aggregate and the matrix for strength in tension, compression, and shear. Half of the samples were soaked in water for twenty-four hours prior to testing. The different modes of failure are analyzed to determine their influence on cracking in asphalt concrete. This chapter describes the results for the matrix tests developed for this study.

6.2 Matrix Tension Test

The samples are tested in tension at a strain rate of 0.05 in/min. (1.27 mm/min). The samples failed at the lift interfaces. Figures 6.1(a) and 6.1(b) are the load versus displacement curves for dry and wet samples. The dry sample withstood a slightly higher load than the wet sample. It can also be seen from the curves that in the dry sample at

120 lbf the data points become more spaced, indicating a greater strain rate. This increase in the strain rate is not present in the wet sample.

6.3 Matrix Compression Test

The samples were tested at a constant strain rate of 0.05 in/min in compression. The samples initially bulged and then fractured along a diagonal plane as normally seen in soil testing. Figures 6.2(a) and 6.2(b) are the load versus displacement curves for the dry and wet sample.

It can be seen from the graphs that the wet sample sustained a significantly higher load than the dry sample. Total load is carried by the coated aggregate and the pore water inside the sample. Upon nearing maximum load, a pressure level inside the sample is achieved beyond which water can no longer stay inside the sample. This pressure is termed the exudation pressure. During the test of the wet sample water could be seen leaving the sample from the base and the side. Figure 6.3 shows the exudation of water from the wet sample during testing.

6.4 Aggregate Pull-off Test

Figures 6.4(a) and 6.4(b) show stress versus strain curves for dry and wet samples. Both curves exhibit a couple thousandths of an inch of displacement and then drop quickly after the ultimate load. The slopes of the cures appear similar, although the load for the dry sample is approximately 40 lbf higher that the load for the dry sample at a vertical displacement of 0.002 in. Therefore, the dry sample interface exhibits a higher modulus of elasticity that the wet sample.

It can be noticed by comparison that the strength of the aggregate/matrix interface for the wet sample is approximately half of the strength for the dry sample. This observation alone indicates that wetting significantly reduces the tensile strength of the interface between the aggregate and the matrix.

6.5 Direct Shear Test

The aggregate is loaded with a shear force at a rate of 0.01 in/min. This rate was reduced from 0.05 in/min, as used in the other three tests, in order to increase the test duration for data collection purposes. Figures 6.5(a) and 6.5(b) are the load versus displacement curves for the dry and wet samples. It can be seen from Figure 6.5(a) and 6.5(b) that the wet sample failed at a higher shear load than the dry sample. It can be noted that the amount of displacement during loading for the wet sample is higher than the dry sample.

6.6 Results and Discussion

The load versus displacement curves captured by each test allow for an analysis of stress and strain for each loading condition. Each test is designed to evaluate the matrix material strength in compression, tension, shear, and adhesion to aggregate. Further more each test is conducted on a dry and wet sample to determine the effect of water on each particular mode of failure.

Sample dimensions are necessary in order to determine the stress and strain for each test. After dividing load and displacement by the effective area and length respectively, three

parameters can be determined from the resulting stress versus strain curve. The maximum stress, σ_{max}, is the highest stress the sample experiences during the test. Strain at maximum load, $\varepsilon_{\sigma ma}$, is the amount of strain present at σ_{max}. And the initial modulus of elasticity, E_o, is the initial slope of the stress strain curve. In the following sections these three parameters are discussed for each sample tested.

Maximum Stress

Figure 6.6 shows σ_{max} for each test at both dry and wet conditions. It can be seen that the matrix material has the most strength when loaded in compression. The maximum stress levels for the tension, adhesion, and shear tests are similar when compared to the compression test, indicating that the tension, adhesive and shear strengths of the matrix material are similar.

When the samples are wetted, the compression and shear tests both see a decrease in the maximum stress. The tension and adhesion tests both show an increase in maximum stress.

It is interesting to note that the matrix compression test resulted in shear failure along a 45 degree angle. That being said, a common factor between the direct shear test and the compression test that is not present in the tension and adhesion tests is shear failure.

A similar argument can be posed for the tension and adhesion tests. In both cases the mode of failure is tension. In both cases wetting of the sample lead to a decrease in the

maximum stress. Therefore, it can be said that sample wetting affects a sample in such a way as to decrease the tensile strength.

Strain at Maximum Stress

Figure 6.7 shows the strain for samples of both dry and wet conditions for the matrix compression, matrix tension, interface shear, and aggregate pull-off tests. The figure shows that the adhesion test has the highest strain at maximum stress compared to the other three tests. The compression test has the second highest strain, and the tension and shear tests have similar amounts of strain.

The strain for the adhesion test is significantly higher than the other three tests. This is because although the displacement at maximum stress is small (.005 in) the thickness of the interface is very small. The thickness of the interface is approximated to be twice the film thickness for mix SP-B. By calculation, that value is .000591 in (15 μm).

The effect of sample wetting on the strain at maximum stress is less pronounced than with maximum stress. Figure 6.7 shows that the strain increased for wet samples in the shear and compression tests, and not in the tension and adhesion tests. An increase in strain in the wetted samples is and indication that the wetting process softens the binder.

Initial Modulus of Elasticity

Figure 6.8 shows the initial moduli for each test sample at both dry and wet moisture conditions. The values for the adhesion test are not comparable in the chart due to the

fact that these values are significantly lower than those for the tension, compression, and shear tests. The small E_o values for the adhesion test result from high strain at the interface between the aggregate and matrix material.

Figure 6.8 shows that the E_o values for the matrix material in tension, compression, and shear are between 20 kpsi and 30 kpsi. Upon wetting, the samples used in the tension and compression tests show an effect due to the moisture, although the shear samples do not indicate as great as an effect. The wet sample in the tension test shows an increase in the initial modulus of elasticity, but the converse applies for the tension test. An increase in the initial modulus of elasticity indicates a stiffening of the material in question. Therefore, the increase in E_o for the wet sample in tension indicates that the sample has stiffened, while the wet sample in compression has softened. This result demonstrates that a moisture damaged binder inside a asphalt concrete mix behaves differently in compression than in tension.

6.7 Conclusions

- The matrix material has more strength in compression than it does in tension.
- The maximum stress for each test increased for wet samples where shear is the primary mode of failure (compression test and direct shear test) and decreased for wetted samples where tension is the primary mode of failure (matrix tension test and aggregate pull-off).

- Similar to the maximum stress, the strain at max stress also increased for wet samples in tests where shear is the primary mode of failure, and decreased for wet samples in tension.
- The adhesion test showed that the interface has an extremely high strain. This result is due to the small thickness of the interface.
- Due to the high strain in the adhesion test, the initial modulus of elasticity is very low for the adhesion test samples.
- Each test showed a decrease in E_o for wet samples except the tension test.

Chapter 7

Conclusions

This study described the testing and analysis of cracking in asphalt concrete samples in the laboratory. Semi-circular notched specimens were prepared using a Superpave Gyratory Compactor and a water-cooled masonry saw. Samples were prepared with varying material properties including notch type, air void content, mix type, and moisture condition. The specimens were tested in three point bending and a crack was initiated at the notch tip located in the center of the flat edge of the specimen. Load and horizontal displacement data at different locations by LVDTs on the specimen were collected in real time. The resulting load versus displacement curves for each specimen yielded parameters that were analyzed for their effectiveness in characterizing crack initiation and propagation in asphalt concrete. Once the most effective parameters were identified, cracking in three mix types was analyzed to determine which mix type is least susceptible to crack initiation and propagation. Observations in the crack pathway gave way to several experiments described in chapter six which had the purpose of determining the bond strength within different phases of asphalt concrete. The major conclusions from each portion of this entire study are summarized below.

Chapter four showed that basic parameters extracted from the load displacement curve may be used to describe cracking behavior in asphalt concrete. The ultimate load (P_{ult}) evinces increased crack initiation resistance in samples with aggregate notch tips as compared to mastic and interface notch tips. Furthermore, P_{ult} clearly demonstrates the increase in strength in wet samples in comparison to dry samples.

The parameters used to evaluate crack propagation were also successful in showing changes due to specimen properties. The crack velocity is able to demonstrate increased cracking in samples with high air void percentage. The slope of the crack propagation curve (θ) revealed that damage due to crack propagation is more extensive in wet samples.

The work described in chapter five used crack initiation and crack propagation parameters to investigate cracking in three different Superpave mixes with a wider range of air voids. The study showed that air voids had little effect on crack initiation and ultimate strength of a specimen, but cracks propagated faster in specimens with higher air voids. Wet samples were shown to resist failure due to cracking by exhibiting increased ductility. Cracking caused more damage in coarser mixes due to increased interface cracking.

These results are backed up by the conclusions drawn from the matrix laboratory tests described in chapter six. The interface phase of the asphalt concrete mix in tension showed the lowest strength of all modes of failure tested.

In summary, the primary contributions of this study are:

- Wet samples sustained more load before crack initiation than dry samples. Further study is required to determine whether or not this result stems from sample geometry.

- Wet samples showed slower cracks than dry samples, which suggests that wet pavements will have a longer service life.
- Air voids had no effect on crack initiation and propagation.
- The interface pathway is preferential for crack initiation and propagation.

REFERENCES

AASHTO T 245. "Standard Method of Test for Resistance to Plastic Flow of Bituminous Mixtures Using Marshall Apparatus." *American Association of State Highway and Transportation Officials* (AASHTO), Washington D. C.

AASHTO T 283. "Resistance of Compacted Bituminous Mixture to Moisture Induced Damage for Superpave." *American Association of State Highway and Transportation Officials* (AASHTO), Washington D. C., (2000).

AASHTO T 312. "Standard Method of Test for Preparing and Determining the Density of Hot Mix Asphalt (HMA) Specimens by Means of the Superpave Gyratory Compactor." *American Association of State Highway and Transportation Officials* (AASHTO), Washington D. C.

ASTM D 2726. "Standard Test Method for Bulk Specific Gravity and Density of Non-Absorptive Compacted Bituminous Mixtures." ASTM International, West Conshohocken, PA, www.astm.org.

Aglan, H. (1993) "Evaluation of the Crack Layer Theory Employing a Linear Damage Evolution Approach." *International Journal of Damage Mech*., Vol. 2.

Aglan, H., Othman, A., Figueroa, L., and Rollins, R. (1994) "Effict of styrene-butadiene-styrene block copolymer on fatigue crack propagation behavior of asphalt concrete mixtures." *Transportation Research Record*, Vol. 1417, 178-186.

Anderson, T. L. Fracture Mechanics, Fundamentals and Applications. Taylor and Francis. Boca Raton, FL. (2005).

Bynum, D. Jr., Evertson, J. F., Eskew, L. C., and Fleisher, H. O. (1973) "Mechanical Properties of Plasticized Bituminous Concrete." *Journal of the Institute of Petroleum* Vol. 59(569)

Dongre, R., Sharma, M. G., Anderson, D. A. (1989) "Development of fracture criterion for asphalt mixes at low temperatures." *Transportation Research Record*, Vol. 1228, 94–105.

Hofman, R., Oosterbaan, B., Erkens, S. M. J. G., van der Kooij, J. (2003) "Semi-circular bending test to assess the resistance against crack growth." *Proceedings of the 6th R1LEM Symposium on Performance Testing and Evaluation of Bituminous Materials, Zurich, Switzerland*. pp. 257-263.

Huang, B., Shu, X., Zuo, G. "Laboratory Evaluation of Semi-Circular Bending Tensile Strength Test for HMA Mixtures." *Proceedings of the Geo-Congress 2005 Conference, (2005)*.

Huang, Y. Pavement Analysis and Design. Prentice Hall. Upper Saddle River, New Jersey. (1992).

Jacobs, M. M. J., Hopman, P. C., Molenaar, A. A. A. (1996) "Application of fracture mechanics principles to analyze cracking in asphalt concrete." *Asphalt Paving Technology*, Vol. 65, 1-39.

Krans, R., Tolman, F., Van de Ven, M. F. C. (1996) "Semi-circular bending test: A practical crack growth test using asphalt concrete cores." *Proceedings of the 3rd International RILEM Conference on Reflective cracking in pavements - design and performance of overlay systems*. France, October 1996.

Li, X., and Marasteanu. M. (2004) "Evaluation of Low Temperature fracture Resistance of Asphalt Mixture Using the Semi-Circular Bend Test." *Journal of the Association of Asphalt Paving Technologists*, Vol. 73: 401-426.

Li, Y. and Metcalf, J. B. (2002) Crack Initiation Model From Asphalt Slab Tests. *Journal of Materials in Civil Engineering,* Vol. 14(4): 303-310.

Masad, E., et al. Internal Structure Characterization of Asphalt Concrete Using Image Analysis. *Journal of Computing in Civil Engineering*, *ASCE,* Vol. 13(2), pp. 88-95, (1999).

Majidzadeh, K. et al. (1976) "Application of fracture mechanics for improved design of bituminous concrete." Rep. FHWA-rd-76-91 Vol. 1-2. Federal Highway Administration, Washington, D.C.

Mobasher, B., Mamlouk, M. S., Lin, H. (1997) "Evaluation of crack propagation properties of asphalt mixtures." *Journal of Transportation Engineering*, Sep./Oct., pp 405-413.

Molennar, A., Scarpas, A., Liu, X, and Erkens, G. (2002) "Semi Circular Test; Simple but Useful." *Journal of the Association of Asphalt Paving Technologists*, Vol. 71.

Mull, M. A., Stuart, K., Yehia, A. (2002) "Fracture resistance characterization of chemically modified crumb rubber asphalt pavement." *Journal of Materials Science*, Vol. 37, 557-566.

Rice, J. R. (1968) "A path independent integral and the approximate analysis of strain concentration by notches and cracks." *Journal of Applied Mechanics*. Vol. 35, 379–386.

Roberts, F. L., Kandhal, P. S., et al. Hot Mix Asphalt Materials, Mixture, Design, and Construction. NAPA Research and Education Foundation. Lanham, Maryland 1996.

Roque, R., Birgisson, B., Sangpetngam, B., and Zhang, Z. (2001). Hot Mix Asphalt Fracture Mechanics : A Fundamental Crack Growth Law for Asphalt Mixtures. *Journal of the Association of Asphalt Paving Technologist*, Vol.70, 816-827.

Roque, R., Zhang, Z. and Sankar, B. (1999) "Determination of Crack Growth Rate Parameters of Asphalt Mixtures Using the Superpave IDT." *Journal of the Association of Asphalt Paving Technologists*, Vol. 68, 404-433.

Van de Ven, M., de Fortier Smit, A., and Krans. R. (1997) "Possibilities of a Semi-Circular Bending Test." *Proceedings of the Eighth International Conference of Asphalt Pavements*, Vol. 2: 939-950, Seattle, WA.

Wagoner, M. P., et al. (2005) Disc-shaped Tension Test for Asphalt Concrete Fracture. *Experimental Mechanics*, Vol. 45, No. 3. pp. 270-277.

Wagoner, M. P., Buttlar, W. G., and Paulino, G. H. (2005a) "Development of a single-edge notched beam test for ashpalt concrete mixtures." *Journal of Testing and Evaluation*, Vol. 33(6), 452-459.

Wagoner, M. P., Buttlar, W. G., Paulino, G. H., Blankenship, P. (2005b) "Investigation of the fracture resistance of hot-mix asphalt concrete using a disk-shaped compact tension test." *Transportation Research Record*, No. 1929, pp 183-192.

Wu, Z., Mohammod, L. N., Wang, L. B., Mull, M. A. (2005) "Fracture resistance characterization of superpave mixtures using the semi-circular bending test." *Journal of ASTM International*, March, Vol. 2(3), pp 1-15.

Zhang, Z., et al. (2001) "Evaluation of Laboratory Measured Crack Growth Rate for Asphalt Mixtures", *Transportation Research Record,* 1767, 67-75.

Table 3.1 Reliability Study Analysis

Sample ID	Ultimate Load (P_{ult}, *lb*)	COD at Ultimate Load (COD_{ult}, in)	Crack Initiation Potential (U, lbxin)	Fracture Load (P_f, lb)	Slope of Crack Propagation Curve (θ, lb/0.035 in)	Initial Crack Velocity (v, in/min)
Wet 1	471	0.0173	9.2	392	114	0.33
Wet 2	397	0.0169	5.9	320	111	0.32
Wet 3	464	0.0193	7.5	406	102	0.26
Average	444	0.0178	7.5	373	109	0.30
Standard Deviation	47	0.0013	1.7	46	6	0.04
Coef. of Variance (%)	11	7	22	12	6	13
Dry 1	496	0.0229	10.8	482	63	0.43
Dry 2	471	0.0195	7.3	453	57.9	0.48
Dry 3	523	0.0204	11.5	504	50.2	0.51
Average	497	0.0210	9.9	480	57	0.47
Standard Deviation	26	0.0018	2.3	26	6	0.04
Coef. of Variance (%)	5	8	23	5	11	9

Table 4.1 Test Matrix A

Mix Type	Air Voids	Condition	Crack Location	Sample
Superpave SP-B	4% 7%	Wet Dry	Aggregate Mastic Interface	Two Replicates

Test Matrix =1 Mix x 2 Air Voids x 2 Moisture Conditions x 3 Crack-tip Locations x 2 Replicates =24 Specimens

Table 5,1 Test Matrix B

Superpave Mix Type	Air Voids	Condition
SP-B SP-C SP-III	<4% 4%<e<7% >7%	Wet Dry

Test Matrix =3 Mix x 3 Air Voids x 2 Moisture Conditions
=18 Samples

Table 3 Regression equations and R-squared values for parameters P_{ult} and P_{int}

	Ultimate Load, P_{ult}	Crack Initiation Load, P_{int}
Wet and Dry	$y = 0.4437x^2 - 12.663x + 348.21$ $R^2 = 0.1674$	$y = 1.6727x^2 - 27.707x + 335.64$ $R^2 = 0.2498$
Dry	$y = 0.2967x^2 - 6.7651x + 306.62$ $R^2 = 0.1146$	$y = 0.0679x^2 - 5.2799x + 271.71$ $R^2 = 0.1516$
Wet	$y = 3.8656x^2 - 55.134x + 453.41$ $R^2 = 0.4717$	$y = 1.264x^2 - 30.332x + 354.54$ $R^2 = 0.4823$

Table 5.3 Cracking and loading parameters for each sample

		Air Voids	Moisture	COD_{ult}	P_{ult} (lb)	P_{int} (lb)	P_{ult}-P_{int}
SP-B	e<4	4.6	DRY	0.084	283	240	43
		4.6	WET	0.053	309	256	53
	4<e<7	6.1	DRY	0.012	261	244	17
		5.6	WET	0.065	267	230	37
	e>7	9.9	DRY	0.016	286	226	60
		9.1	WET	0.040	156	142	14
SP-C	e<4	1.1	DRY	0.017	337	308	29
		1.5	WET	0.028	302	240	61
	4<e<7	4.2	DRY	0.028	263	227	36
		5.9	WET	0.069	277	144	133
	e>7	9.5	DRY	0.014	266	221	45
		10.4	WET	0.028	301	240	61
SP-III	e<4	1.8	DRY	0.002	306	304	2
		3.5	WET	0.009	432	375	56
	4<e<7	7.1	DRY	0.013	306	227	79
		5.1	WET	0.009	321	239	82
	e>7	9.6	DRY	0.007	229	222	7
		9.2	WET	0.011	351	302	49

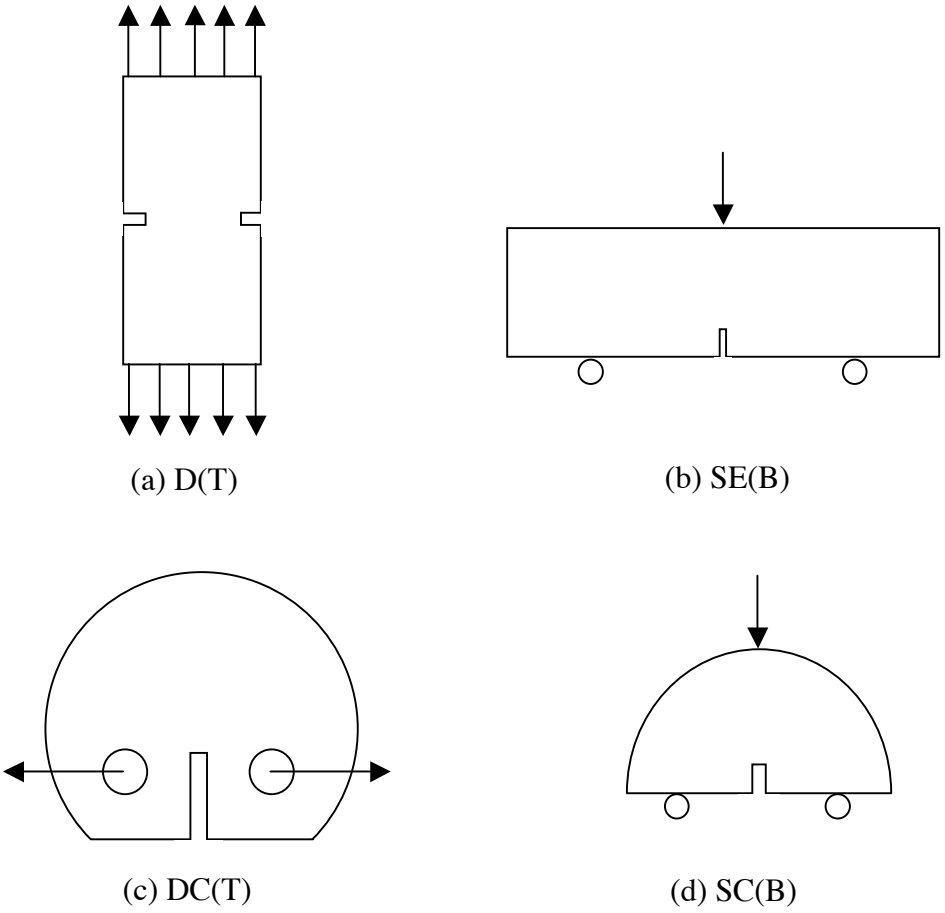

Figure 2.1 Common specimen geometries for the study of fracture in asphalt concrete

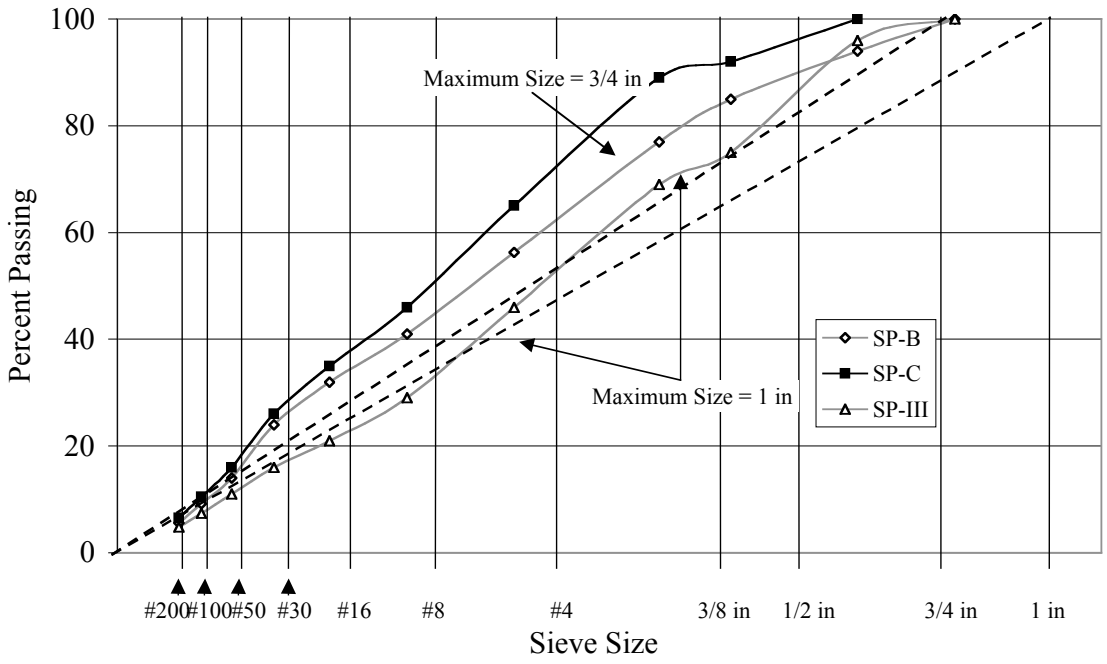

Figure 3.1 Aggregate gradation for Superpave mixes SP-B, SP-C, and SP-III

(a) Gyratory Sample (b) Sliced Sample (c) Notched Samples

Figure 3.2 Notched sample preparation steps

Figure 3.3 Notch tip locations

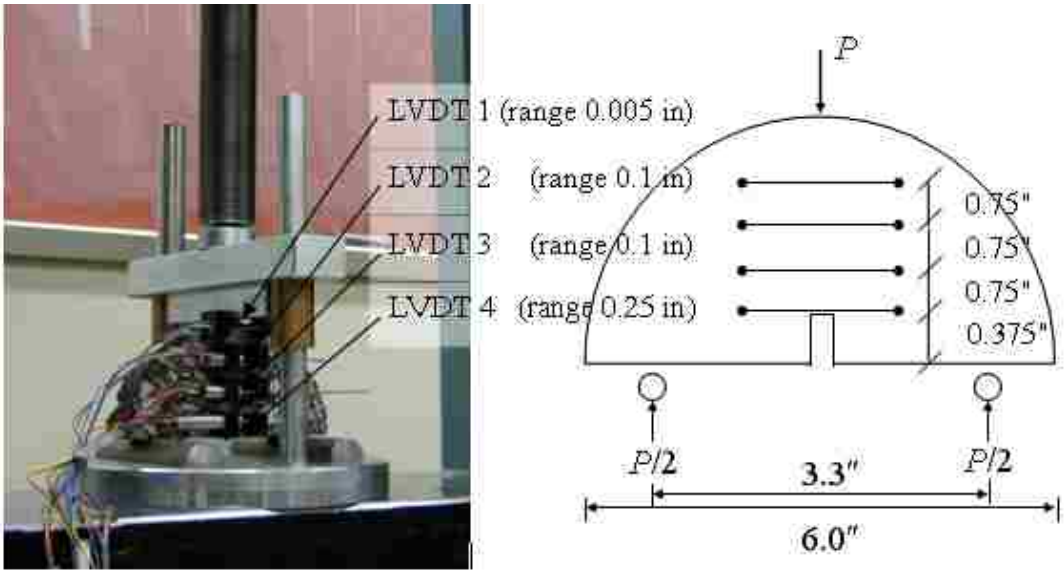

Figure 3.4 Sample loading configuration and LVDT placement

Figure 3.5 Materials for Preparation of Cylindrical Samples

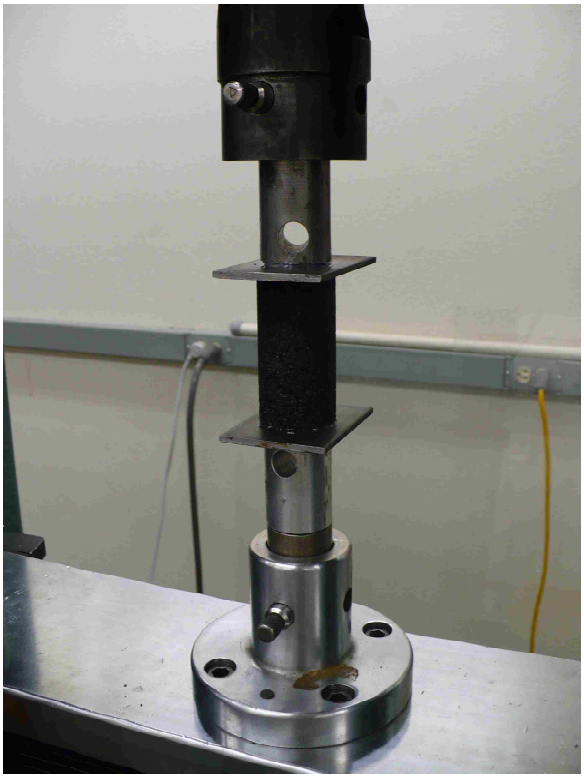

Figure 3.6 Test setup for cylindrical matrix samples

Figure 3.7 Test setup for aggregate/matrix interface in tension

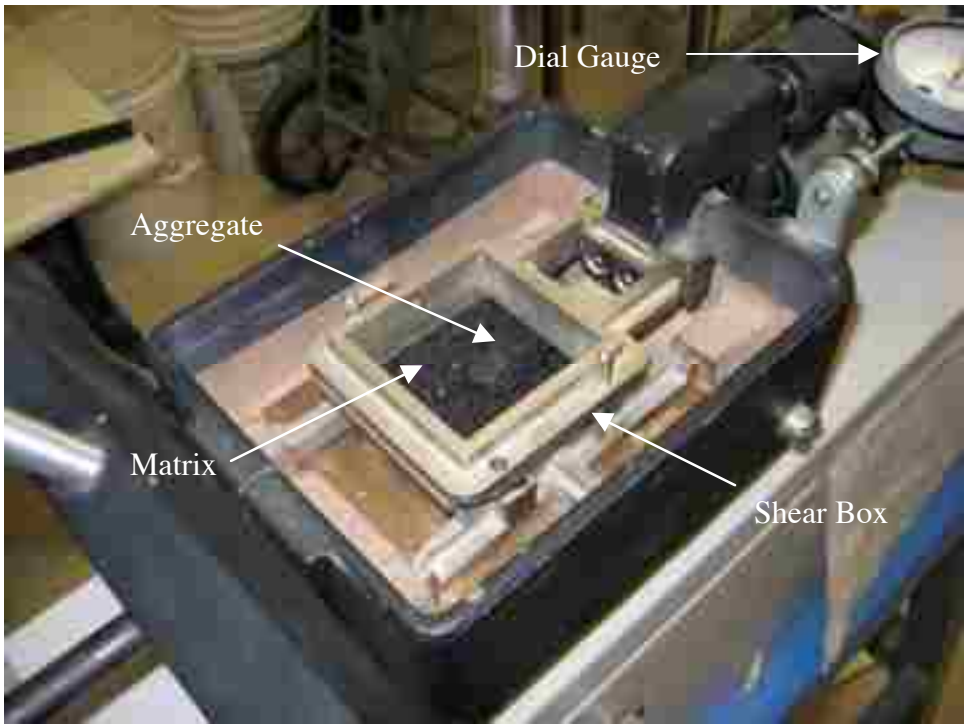

Figure 3.8 Testing configuration for direct shear test of aggregate/matrix interface

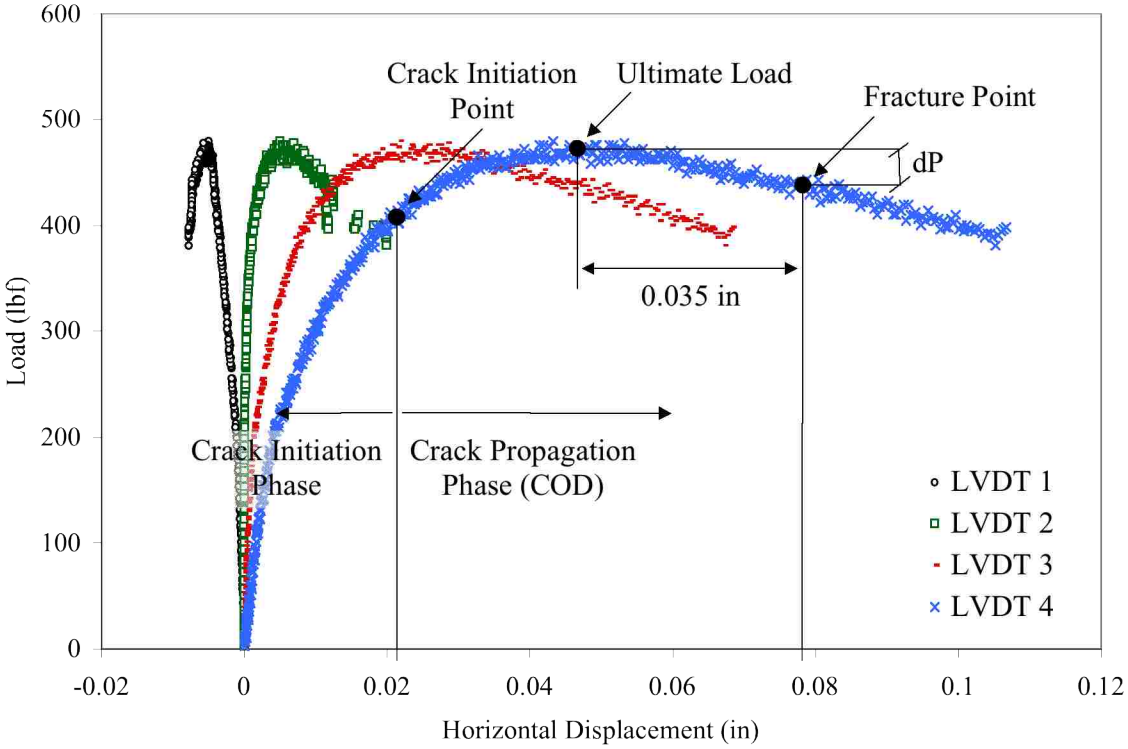

Figure 4.1 Load versus horizontal displacement data for one sample of mix SP-B

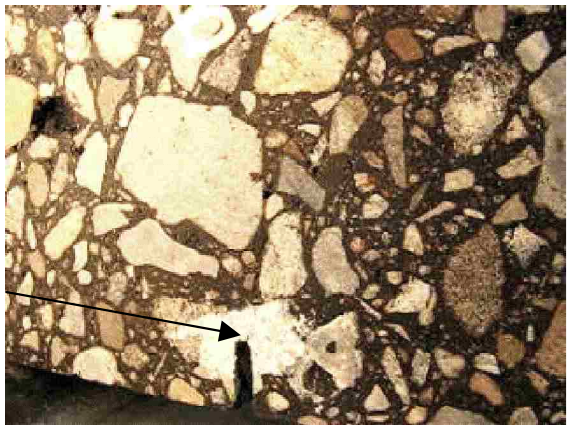

(a) Hairline Crack Initiation

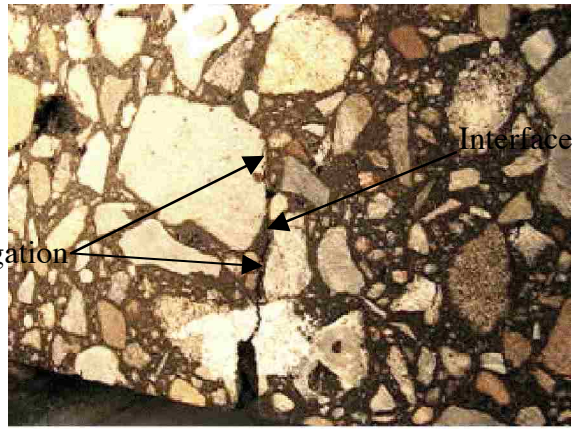

(b) Crack Propagation Along Interfaces

(c) Crack Wandering Through the Mastic

Figure 4.2 Crack propagation path from specimen testing

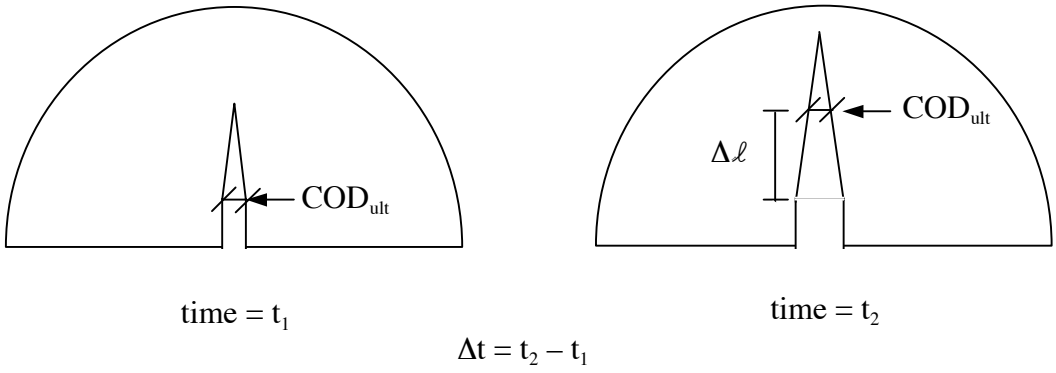

Figure 4.3 Schematic of the locations of same amount of COD_{ult} in Δt time difference

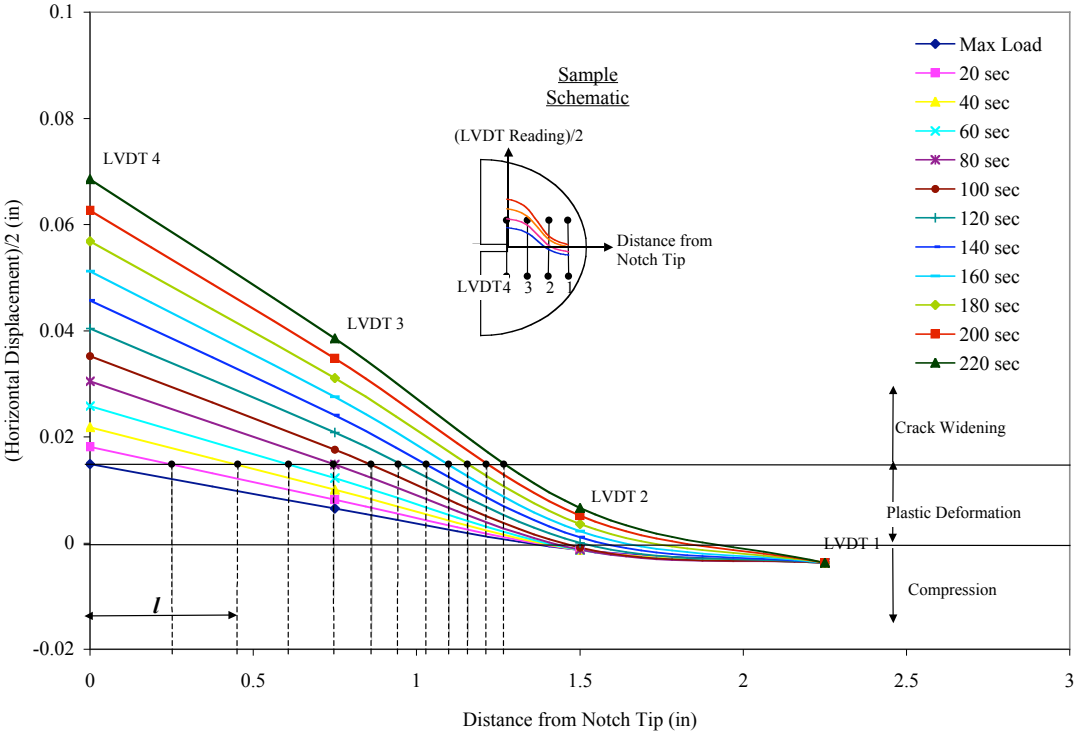

Figure 4.4 LVDT reading vs. distance from notch tip at 20 sec intervals

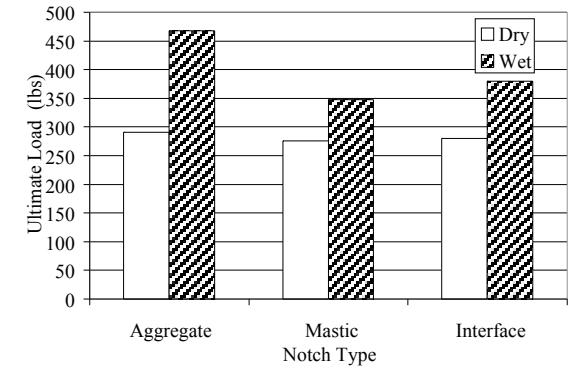

(a) Average, 4% Air Void Ratio

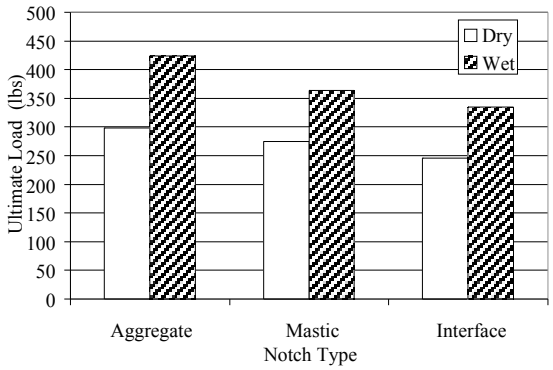

(b) Average, 7% Air Void Ratio

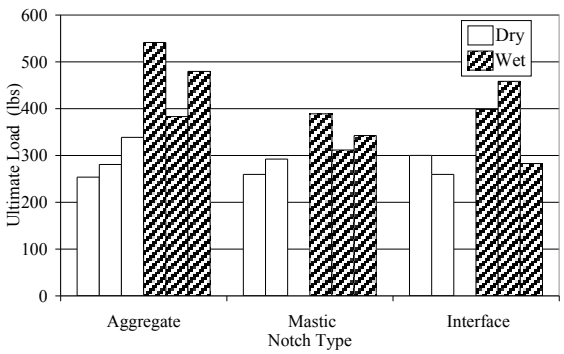

(c) Actual, 4% Air Void Ratio

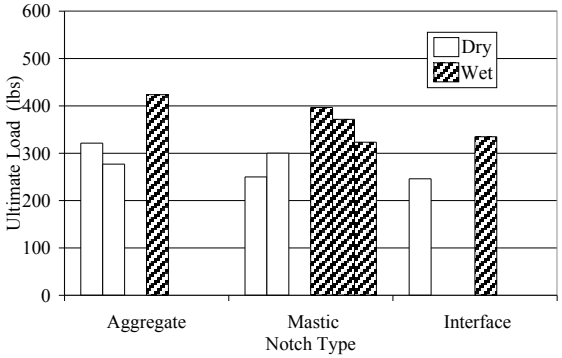

(d) Actual, 7% Air Void Ratio

Figure 4.5 Ultimate load of samples with different notch type

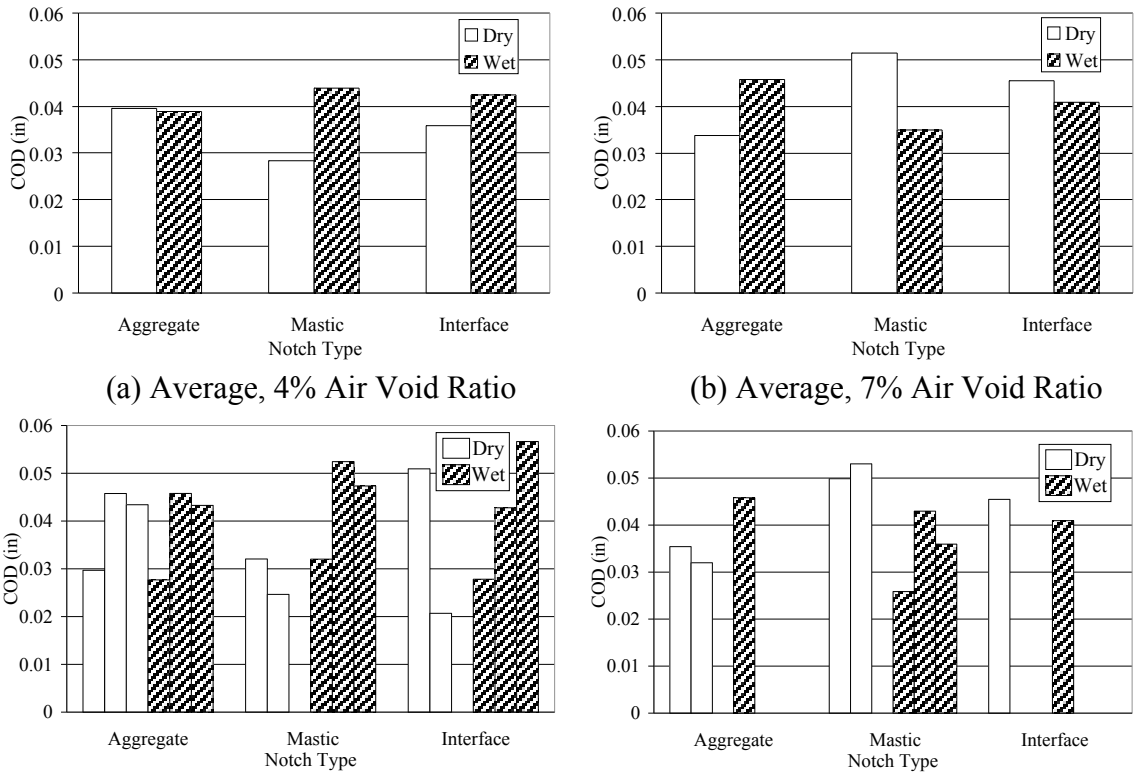

(a) Average, 4% Air Void Ratio

(b) Average, 7% Air Void Ratio

(c) Actual, 4% Air Void Ratio

(d) Actual, 7% Air Void Ratio

Figure 4.6 COD at ultimate load for each notch at wet and dry conditions

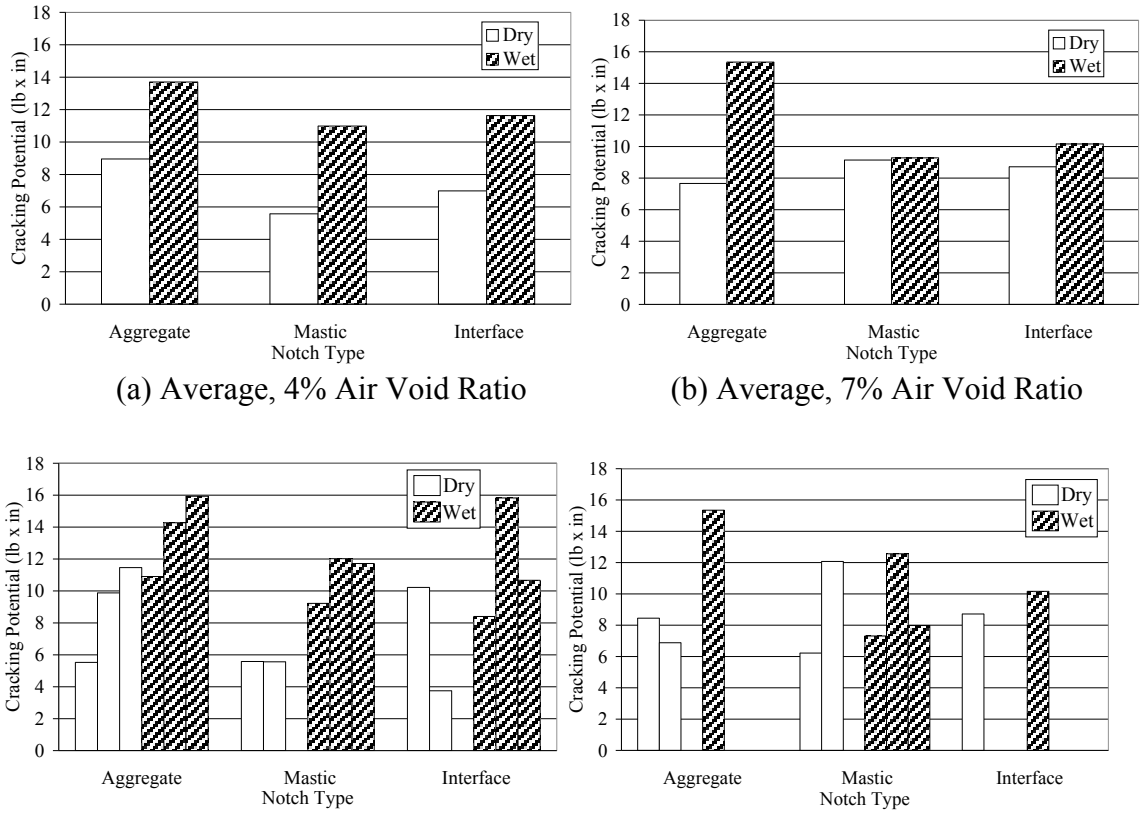

(a) Average, 4% Air Void Ratio (b) Average, 7% Air Void Ratio

(c) Actual, 4% Air Void Ratio (d) Actual, 7% Air Void Ratio

Figure 4.7 Cracking potential for each notch type at wet and dry conditions

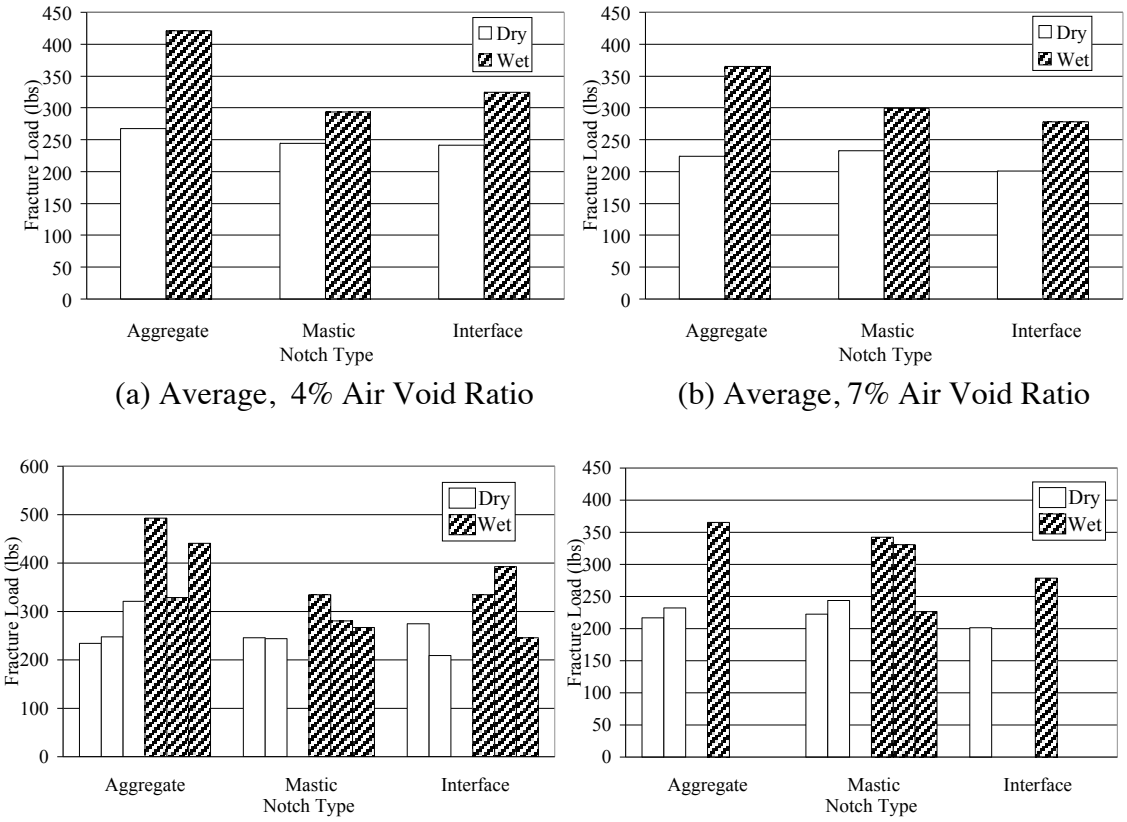

(a) Average, 4% Air Void Ratio

(b) Average, 7% Air Void Ratio

(c) Actual, 4% Air Void Ratio

(d) Actual, 7% Air Void Ratio

Figure 4.8 Fracture load for each notch type at wet and dry conditions

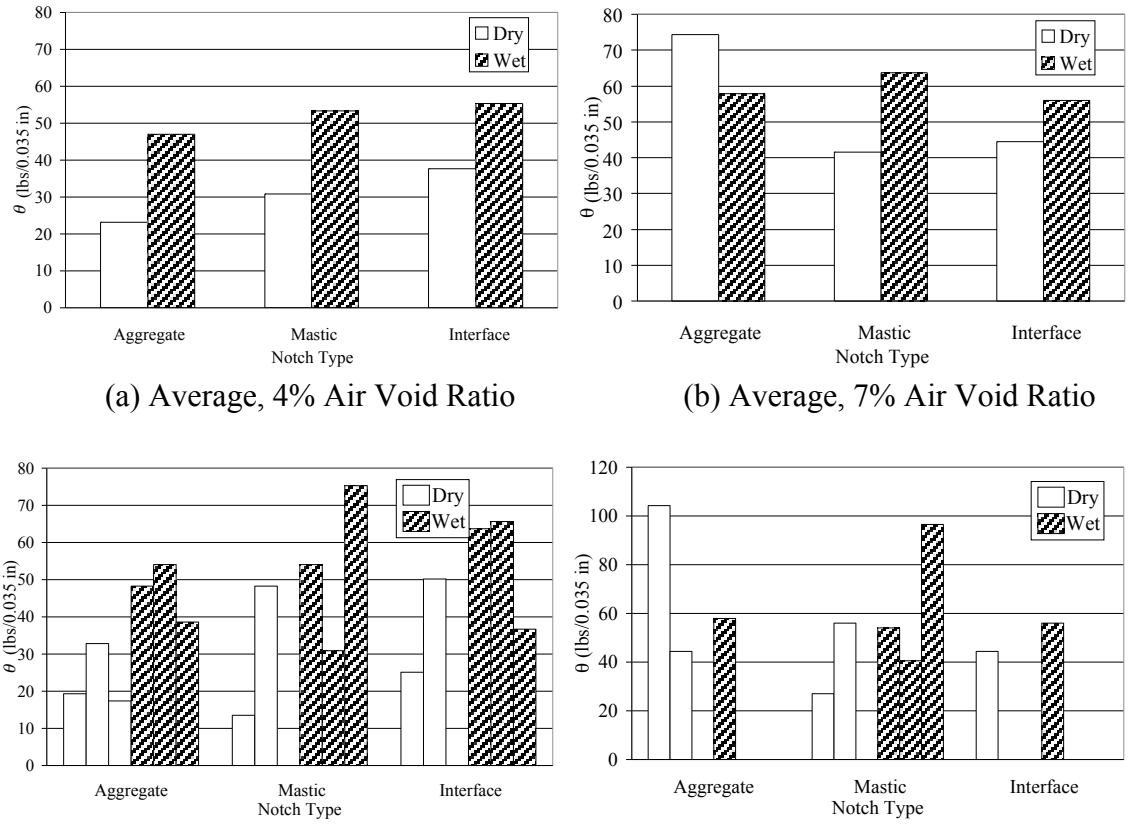

(a) Average, 4% Air Void Ratio

(b) Average, 7% Air Void Ratio

(c) Actual, 4% Air Void Ratio

(d) Actual, 7% Air Void Ratio

Figure 4.9 Slope of the crack propagation curve at wet and dry conditions

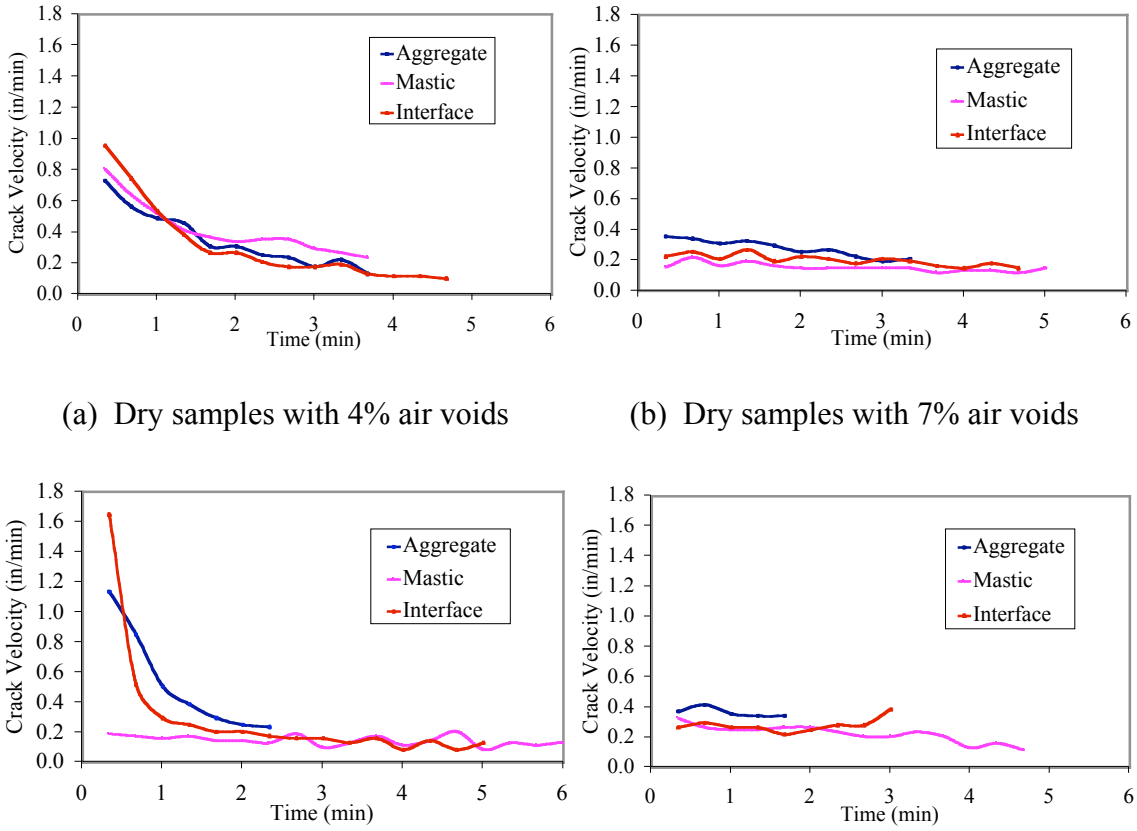

(a) Dry samples with 4% air voids

(b) Dry samples with 7% air voids

(c) Wet samples with 4% air voids

(d) Wet samples with 7% air voids

Figure 4.10 Crack velocity versus time

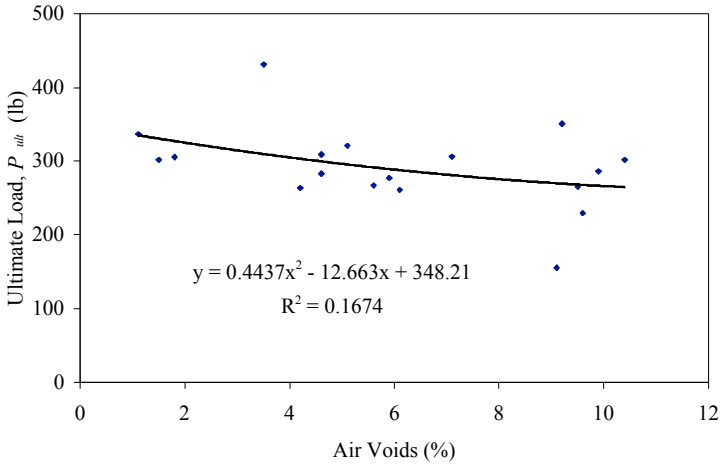

(a) Ultimate load vs. percent air voids

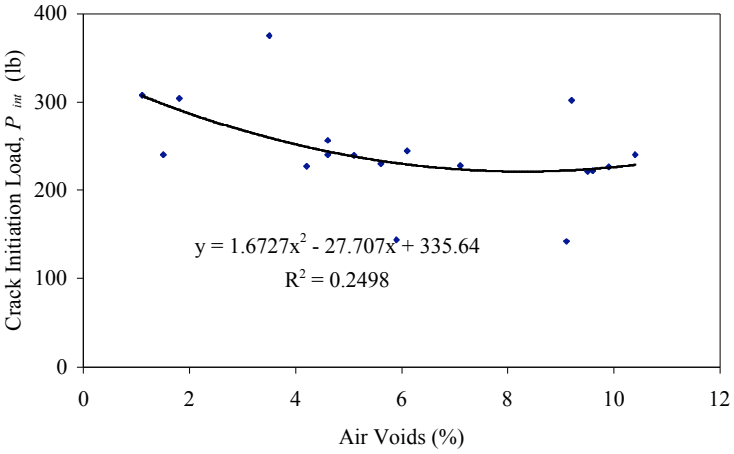

(b) Crack initiation load vs. percent air voids

Figure 5.1 Crack initiation load and ultimate load versus air void percentage

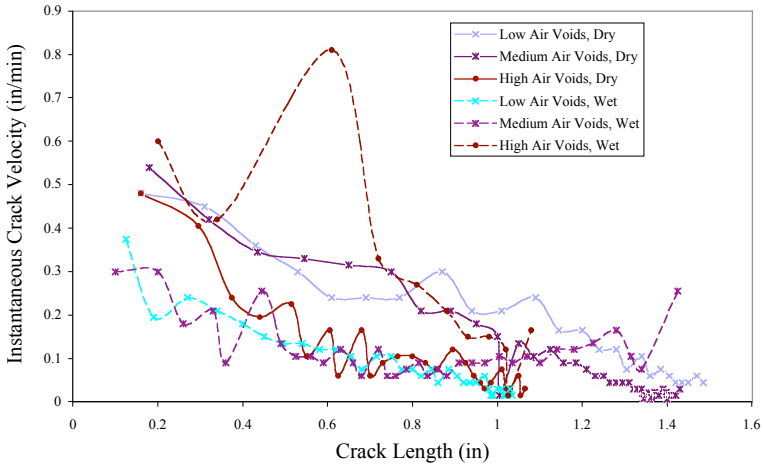

(a) Effect of air voids on crack velocity

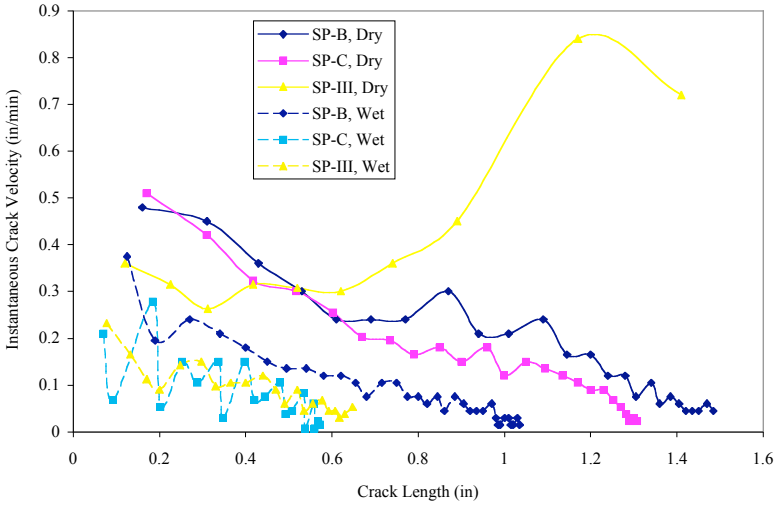

(b) Effect of mix type on crack velocity

Figure 5.2 Crack velocity versus crack length

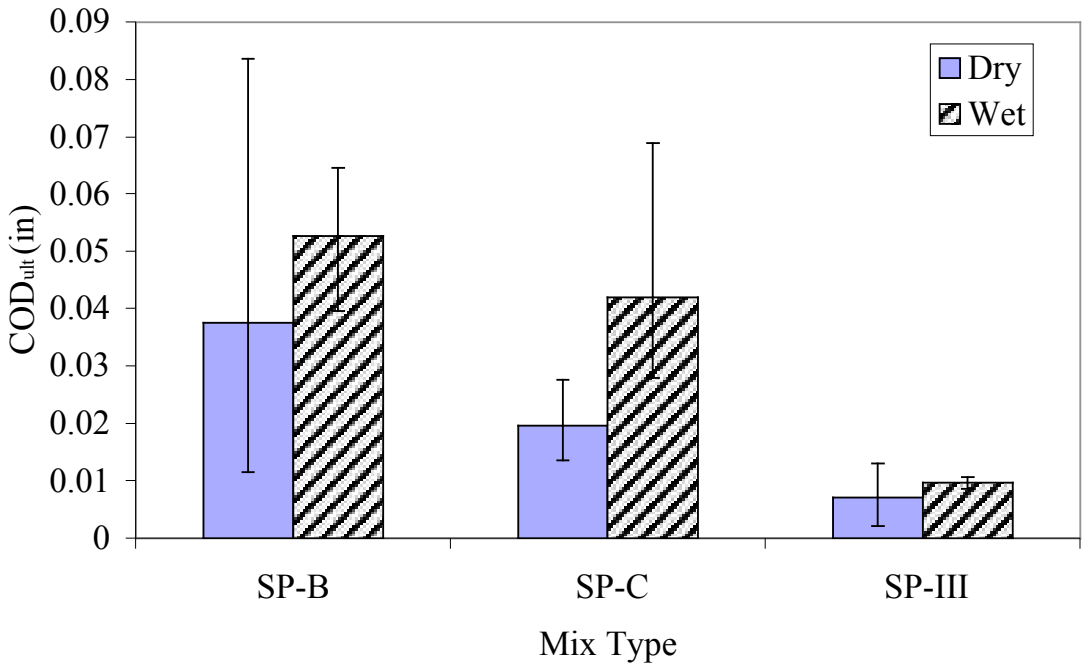

Figure 5.3 Crack opening displacement at ultimate load for dry and wet samples of each mix type

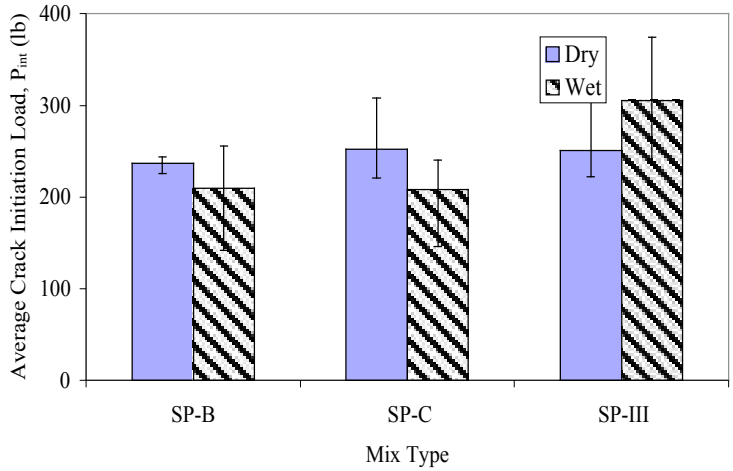

(a) Crack initiation load

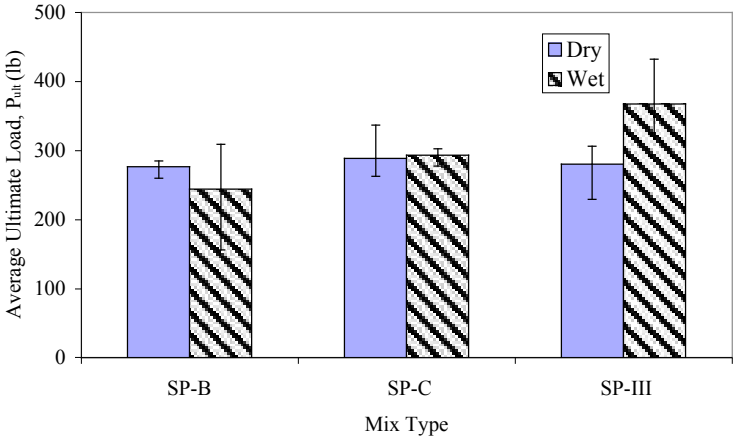

(b) Ultimate load

Figure 5.4 Average crack initiation and ultimate loads for dry and wet samples

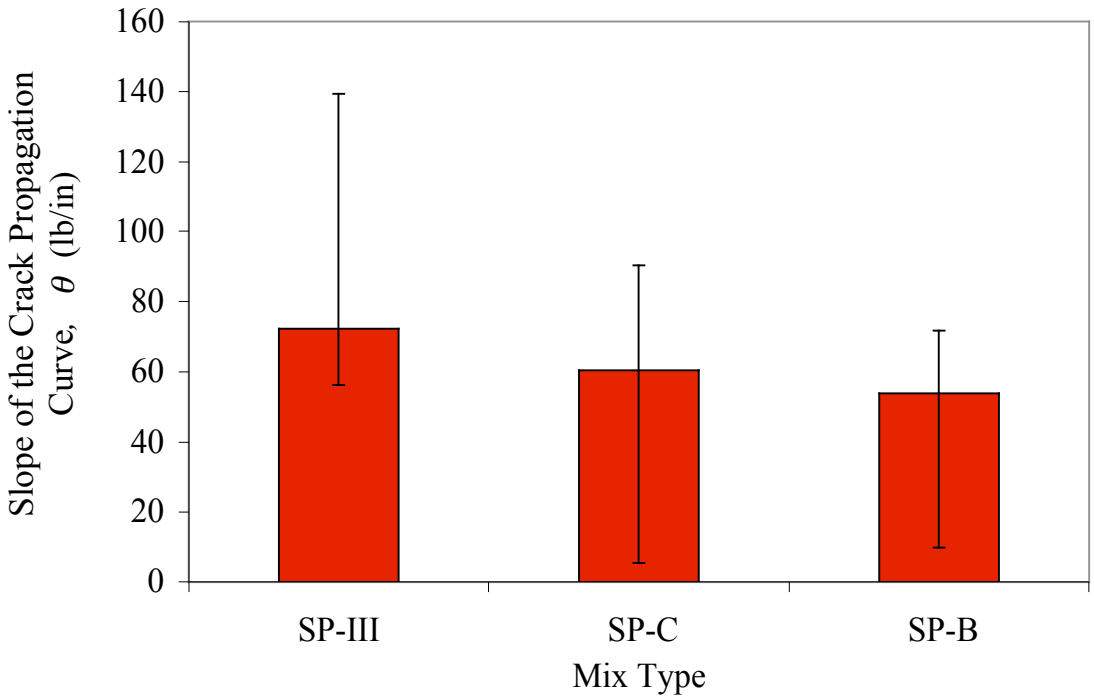

Figure 5.5 Average slope of the crack propagation curve for each Superpave mix type

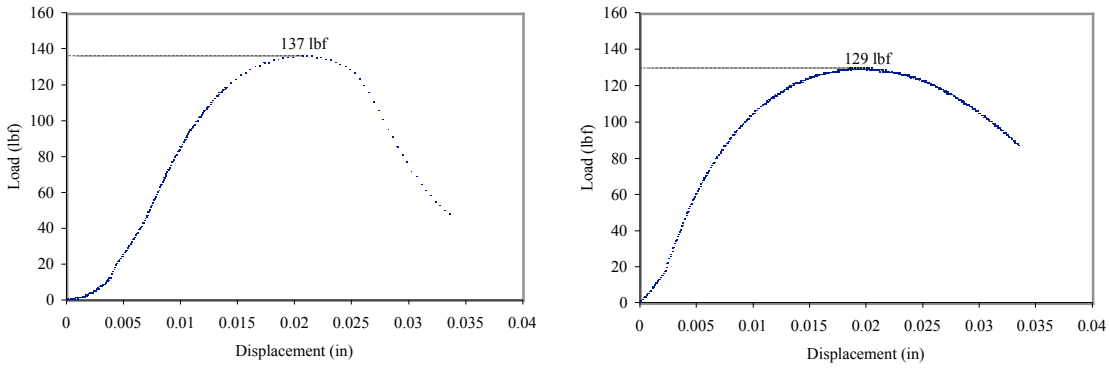

(a) Dry (b) Wet

Figure 6.1 Load versus displacement for cylindrical matrix sample in tension

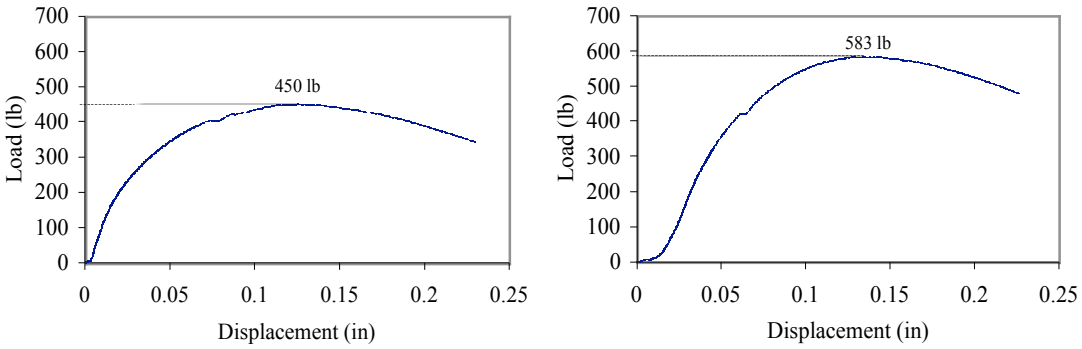

(a) Dry (b) Wet

Figure 6.2 Load versus displacement for dry and wet matrix samples in compression

Figure 6.3 Exudation of water from matrix sample during compression

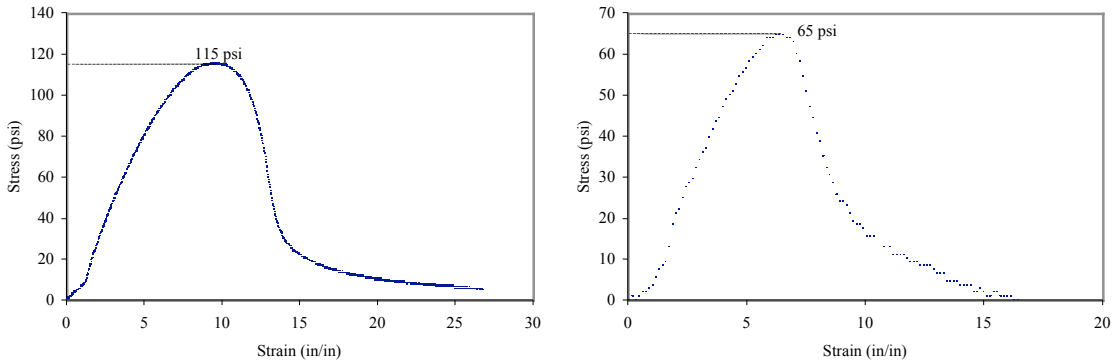

(a) Dry (b) Wet

Figure 6.4 Stress versus strain for aggregate/matrix interface in tension

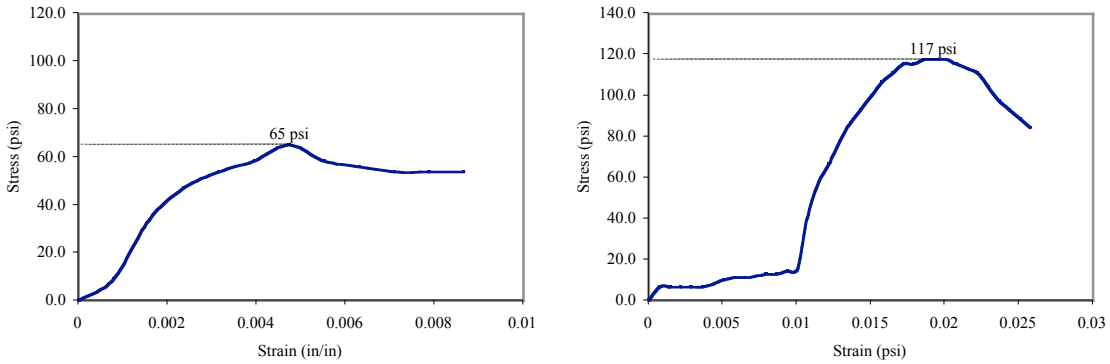

(a) Dry (b) Wet

Figure 6.5 Stress versus strain for the aggregate-matrix interface due to shear

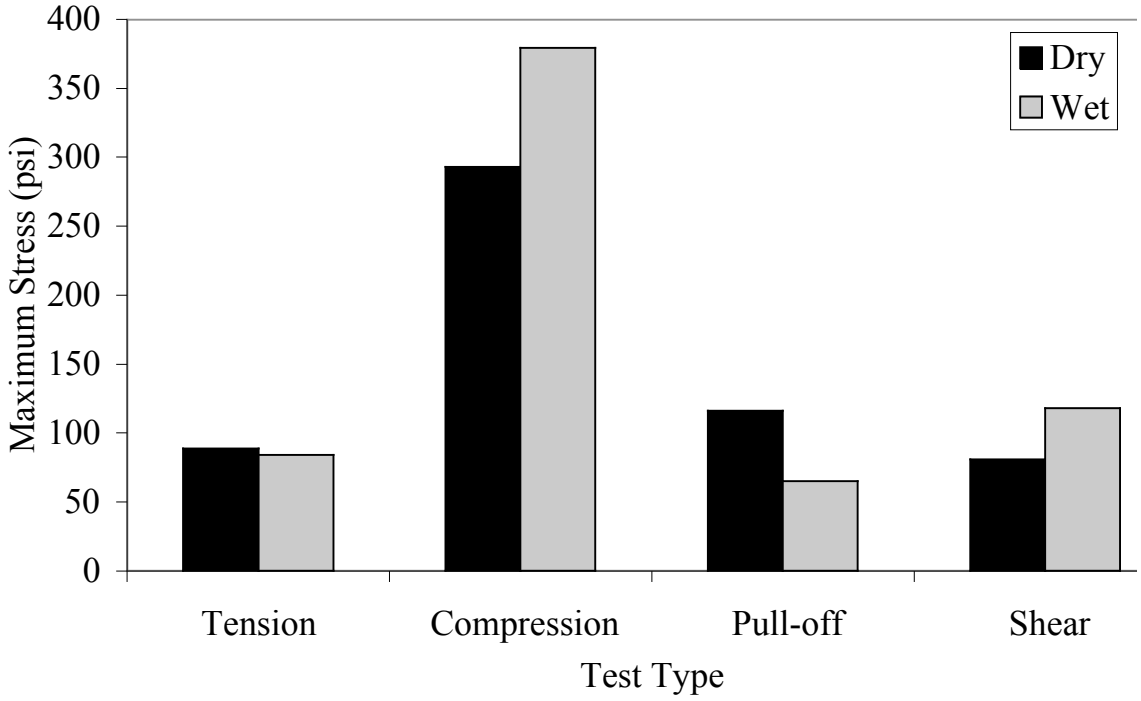

Figure 6.6 Maximum stress for each test type at dry and wet moisture conditions

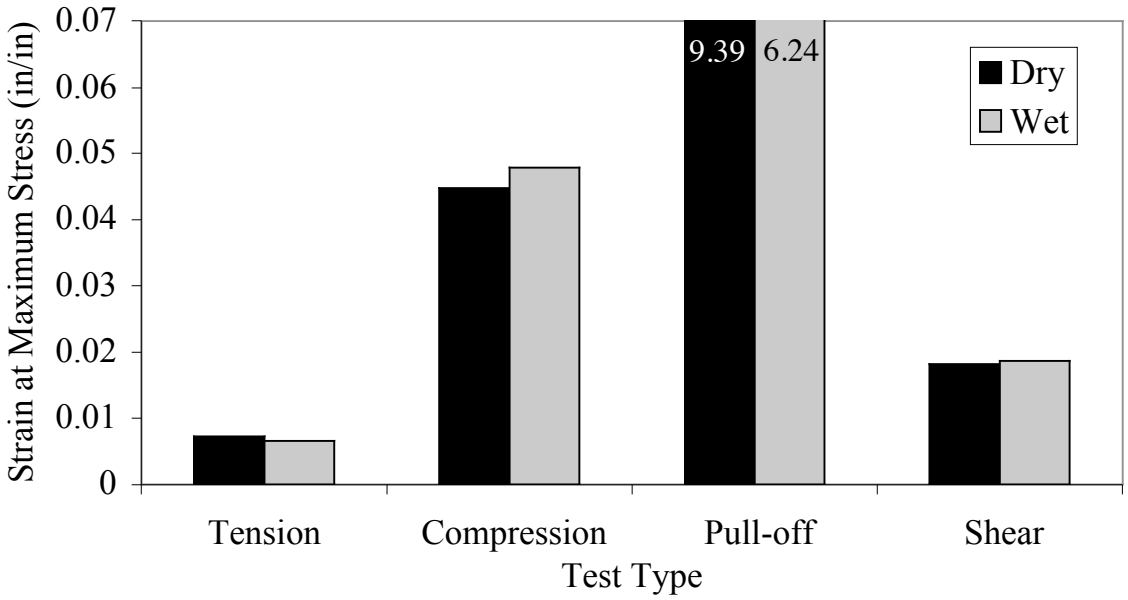

Figure 6.7. Strain at maximum stress for each test at dry and wet moisture conditions

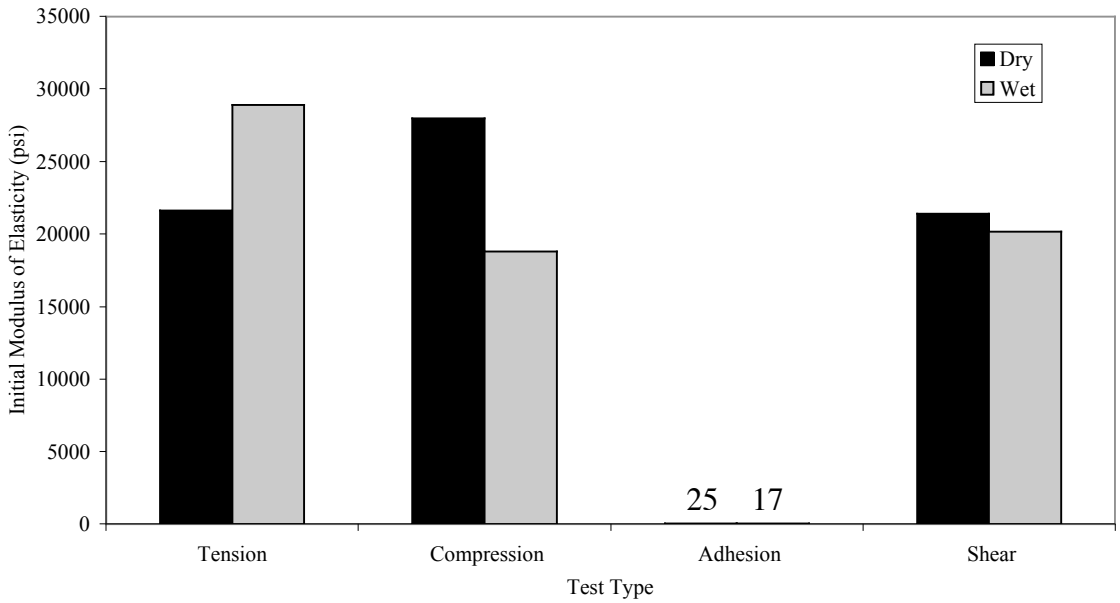

Figure 6.8 Initial modulus of elasticity for each test at dry and wet moisture conditions

Appendix A

LAFARGE NORTH AMERICA
AGGREGATES, CONCRETE & ASPHALT

Product Quality Assurance Department
3/4 inch Bituminous Mix Design Summary Report

7/75/115 Gyrations

Mix Design Number:	B0603-0066			Date Issued:	February 9, 2006
Mix Code Number:	A5637022/A5737022	ESALS:	<3,000,000		
Project Number:	05015	Region:	City Wide	Location:	City of Albuquerque
Control Number:	NA	County:	Bernalillo	Materials Engineer:	Martin Barker
				Date Tested:	2/4/06 -2/9/06

Aggregate

Date of Aggregate Properties Tests: 01/06

Pit or Source: Santa Ana-Placitas-Osuna

Section14,T13N,R4E, Bernalillio County

Aggregate Type: Limestone

Bulk Specific Gravities			
Product	% Used	Bulk SG	Abs%
Rap	15.0%	2.525	1.7
#56	15.0%	2.629	0.8
#7	14.0%	2.618	0.9
CF	40.0%	2.605	1.2
NF	16.0%	2.418	2.1

Asphalt

Supplier/Source: Holly Asphalt

Grade: PG 70-22

Specific Gravity (G_b): 1.034

Mix Type	Combination Used:	Rap	#56	#7	CF	NF		
3/4 inch		15.0%	15.0%	14.0%	40.0%	16.0%	100.0%	Combined Bulk Specific Gravity: 2.566
19 mm								

Sieve Size	Metric / Standard		25 mm / 1"	19 mm / 3/4"	12.5 mm / 1/2"	9.5 mm / 3/8"	2.36 mm / #8	1.18 mm / #16	0.6 mm / #30	0.3 mm / #50	0.75 mm / #200
Gradation Used	% Passing		100	94	85	77	41	32	24	14	5.6
Design Specification Band		CoA SP-B	*100*	*88-96*	*90 max*	*70-85*	*35-49*	*28-40*	*21-31*	*14-23*	*2.0-8.0*
Production Tolerances			100	86-100	77-93	69-85	35-47	26-38	19-29	9-19	2.6-8.6

SUMMARY OF BLEND INFORMATION

Mix Property	Design Data	Design Criteria	Production Criteria	Mix Property	Design Data	Design Criteria	Design Criteria lbs/ft³
% Asphalt (P_{ub})	5.6	n/a	5.1 - 6.1	Bulk Density @ Ndes (75)	2.355	n/a	146.6
(% virgin AC)	89%	75% min					
% Air Voids (V_{al})	4.0	3.5-4.5	3.0 - 5.0	Gmm (T-209)	2.451	n/a	152.6
VMA	13.5	13 - 15	12.5 - 14.5	% Comp. @ Nini (7)	88.1	< 91	
VFA	70.3	68 - 78	68-78	% Comp. @ Nmax (115)	97.4	< 98.0	
Gse	2.670	n/a	n/a	Dust Proportions (D_p)	1.33	0.6 - 1.6	
% Effective AC (P_{be})	4.5	n/a	n/a	% Binder Absorption (P_{ba})	1.24	n/a	

PROPERTIES AT N-DESIGN (75 GYRATIONS)

Percent AC	Maximum Theoretical Unit Weight Gmm	kg/m³	lbs/ft³	Gmb as %Gmm	Bulk Density @ Ndes Gmb	kg/m³	lbs/ft³	Pbe/-200	Percent Air Voids	Percent VMA	Percent VFA
5.2	2.467	2467	153.6	94.6	2.334	2334	145.3	1.5	5.4	13.8	61.0
5.7	2.449	2449	152.4	96.2	2.355	2355	146.6	1.3	3.8	13.5	71.4
6.2	2.431	2431	151.3	97.3	2.367	2367	147.3	1.2	2.7	13.5	80.3
6.7	2.414	2414	150.3	98.3	2.373	2373	147.7	1.1	1.7	13.7	87.6

	°C	°F	Temp Band (°C)	Temp Band (°F)	Tesile Strength Ratio(AASHTO T-283)			
					Dry	Wet	TSR	Minimum Required
Mixing Temp.	164	327	161 - 167	322 - 333				
Molding Temp.	153	307	150 - 155	302 - 311	138 psi	130 psi	93.5%	80.0%
Release to Traffic Temp:		151	Max		951 kPa	896 kPa		

COMPOSITE BLEND AGGREGATE PHYSICAL PROPERTIES

Tests Performed	Design Data	Design Criteria	Tests Performed	Design Data	Design Criteria
ASTM D4791 - Flat & Elongated Pieces	15%	20% max	ASTM C 131, LA Abrasion	27%	40 max
ASTM D1252, Fine Aggregate Angularity	45.1	45 min	ASTM C 88, Soundness Loss	7.2%	15 max
ASTM D 5821, Fractured Faces	100/98	95/90	AASHTO T-90, Plastic Index	SNP	NP
ASTM D 2419, Sand Equivalent	76	45 min	Section 910, Aggregate Index	13.7	N/A
Weight for Gyratory Pucks (grams)	4,625	n/a	Daily Production Gradation Control		Plant Sample From Silo
Ignition Correction Factor	0.17	n/a			

orted By: John Galvin

Tested by: Ray Cruz
Asphalt Lab Technician

STEVEN A. HOOPER NEW MEXICO 7093 REGISTERED PROFESSIONAL ENGINEER

Reviewed by:
Steven A. Hooper; NM Registered Professional Engineer # 7093

Appendix B

LAFARGE NORTH AMERICA
AGGREGATES, CONCRETE & ASPHALT

Product Quality Assurance Department
1/2 inch Bituminous Mix Design Summary Report

7/25/115 Gyrations

Mix Design Number: B0603-0044
Mix Code Number: A5647022/A5747022
Project Number: 06015
Date Tested: 01/16/06 to 01/27/06

ESALS: <3,000,000
Region: City Wide
County: Bernalillo

Date Issued: January 31, 2006
Location: City of Albuquerque
Materials Engineer: Martin Barker

Aggregate

Date of Aggregate Properties Tests:01/06
Pit or Source
Santa Ana-Placitas-Osuna
Section14,T13N,R4E, Bernalillo County

Aggregate Type
Mix Type: Limestone

Bulk Specific Gravities

Product	% Used	Bulk SG	Abs%
Rap	15.0%	2.525	1.7
#6	9.0%	2.621	0.9
#8	8.0%	2.622	1.0
CF	53.0%	2.594	1.3
NF	15.0%	2.481	2.1

Asphalt

Supplier/Source: Holly Asphalt
Grade: PG 70-22
Specific Gravity (G_b): 1.034

	Combination Used:	Rap	#6	#8	CF	NF	
1/2 inch		15.0%	9.0%	8.0%	53.0%	15.0%	100.0%
12.5 mm							

Combined Bulk Specific Gravity: 2.570

Sieve Size	Metric / Standard		19 mm / 3/4"	12.5 mm / 1/2"	9.5 mm / 3/8"	4.75 mm / #4	2.36 mm / #8	1.18 mm / #16	0.6 mm / #30	0.3 mm / #50	0.75 mm / #200
Gradation Used	% Passing		100	92	89	65	46	35	26	16	6.5
Design Specification Band		CoA SP-C	*100*	*88-96*	*90*	*57-75*	*39-58*	*32-48*	*24-38*	*16-27*	*3-10*
Production Tolerances			100	84-100	81-97	57-73	40-52	29-41	21-31	11-21	3.5-9.5

SUMMARY OF BLEND INFORMATION- Calculated (interpolated) from properties at Ndesign

Mix Property	Design Data	Design Criteria	Production Criteria	Mix Property	Design Data	Design Criteria	Design Criteria lbs/ft³
% Asphalt (P_{ub})	5.9	n/a	5.4 - 6.4	Bulk Density @ Ndes (75)	2.343	n/a	145.8
(% virgin AC)	93%	75% min					
Air Voids (V_{al})	4.1	3.5-4.5	3.1 - 5.1	Gmm (T-209)	2.446	n/a	152.3
VMA	14.1	14 - 16	13.1 - 14.1	% Comp. @ Nini (7)	87.5	< 91	
VFA	71.0	68 - 78	66-76	% Comp. @ Nmax (115)	97.1	< 98.0	
Gse	2.675	n/a	n/a	Dust Proportions (D_n)	1.47	0.6 - 1.6	0.67-2.26
% Effective AC (P_{be})	5.0	n/a	n/a	% Binder Absorption (P_{ba})	1.19	n/a	

PROPERTIES AT N-DESIGN (75 GYRATIONS)

Percent AC	Maximum Theoretical Unit Weight Gmm	kg/m³	lbs/ft³	Gmb as %Gmm	Bulk Density @ Ndes Gmb	kg/m³	lbs/ft³	Pbe/-200	Percent Air Voids	Percent VMA	Percent VFA
5.0	2.479	2479	154.3	93.1	2.307	2307	143.6	1.8	6.9	14.8	53.0
5.5	2.461	2461	153.2	94.8	2.332	2332	145.2	1.6	5.2	14.3	63.5
6.0	2.443	2443	152.0	96.1	2.348	2348	146.1	1.4	3.9	14.1	72.6
6.5	2.425	2425	151.0	97.2	2.357	2357	146.7	1.3	2.8	14.2	80.4

	°C	°F	Temp Band (°C)	Temp Band (°F)	Tesile Strength Ratio(AASHTO T-283) Dry	Wet	TSR	Minimum Required
Mixing Temp.	164	327	161 - 167	322 - 333	102 psi	95 psi	93.2%	80.0%
Molding Temp.	153	307	150 - 155	302 - 311	703 kPa	655 kPa		
Release to Traffic Temp:		151	Max					

COMPOSITE BLEND AGGREGATE PHYSICAL PROPERTIES

Tests Performed	Design Data	Design Criteria	Tests Performed	Design Data	Design Criteria
ASTM D4791 - Flat & Elongated Pieces	9%	20% max	ASTM C 131, LA Abrasion	26%	40 max
ASTM D1252, Fine Aggregate Angularity	45.3	45 min	ASTM C 88, Soundness Loss	3.2%	15 max
ASTM D 5821, Fractured Faces	97/93	95/90	AASHTO T-90, Plastic Index	NP	NP
ASTM D 2419, Sand Equivalent	62	45 min	Section 910, Aggregate Index	10.3	N/A
Weight for Gyratory Pucks (grams)	4,750	n/a	Daily Production Gradation Control	Plant Sample From Silo	
Ignition Correction Factor	-0.16	n/a			

Tested By: John Galvin
Tested by: Ray Cruz
Asphalt Lab Technician

Reviewed by:
Steven A. Hooper, NM Registered Professional Engineer # 7093

STEVEN A. HOOPER NEW MEXICO 7093 REGISTERED PROFESSIONAL ENGINEER

Appendix C

LAFARGE NORTH AMERICA
AGGREGATES, CONCRETE & ASPHALT

Product Quality Assurance Department
3/4 inch Bituminous Mix Design Summary Report

8/100/160 GYRATIONS

Mix Design Number:	B0603-0102			Date Issued:	April 27, 2006
Mix Code Number:	A5637628/A5737628	ESALS:	3,000,000<30,000,000		
Project Number:	06015	Region:	City Wide	Location:	City of Albuquerque
Control Number:	NA	County:	Bernalillo	Materials Engineer:	Martin Barker
				Date Tested:	2/20/06-3/16/06

Aggregate

Date of Aggregate Properties Tests.01/06

Pit or Source: Santa Ana-Placitas-Osuna

Section14,T13N,R4E, Bernalillio County

Aggregate Type: Limestone

Bulk Specific Gravities			
Product	% Used	Bulk SG	Abs%
Rap	15.0%	2.525	1.7
#56	10.0%	2.629	0.8
#6	20.0%	2.621	0.9
#8	15.0%	2.622	1.0
CF	40.0%	2.605	1.2
	0.0%		

Asphalt

Supplier/Source: Holly Asphalt

Grade: PG 76-28

Specific Gravity (G_b): 1.029

Mix Type: 3/4 inch / 19 mm

Combination Used:	Rap	#56	#6	#8	CF		100.0%
	15.0%	10.0%	20.0%	15.0%	40.0%	0.0%	

Combined Bulk Specific Gravity: 2.601

Sieve Size	Metric / Standard		25 mm / 1"	19 mm / 3/4"	12.5 mm / 1/2"	9.5 mm / 3/8"	2.36 mm / #8	1.18 mm / #16	0.6 mm / #30	0.3 mm / #50	0.75 mm / #200
Gradation Used	% Passing		100	96	75	69	29	21	16	11	4.8
Design Specification Band		CoA SP-III	*100*	*89-96*	*90 max*	*64-85*	*23-32*	*12-22*	*8-17*	*5-14*	*3.0-8.0*
Production Tolerances			100	88-100	67-83	61-77	23-35	15-27	11-21	6-16	1.8-7.8

SUMMARY OF BLEND INFORMATION

Mix Property	Design Data	Design Criteria	Production Criteria	Mix Property	Design Data	Design Criteria	Design Criteria lbs/ft³
% Asphalt (P_{ub})	5.3	n/a	4.8 - 5.8	Bulk Density @ Ndes (100)	2.350	n/a	146.3
(% virgin AC)	89%	75% min					
% Air Voids (V_{ni})	4.0	3.5-4.5	3.0 - 5.0	Gmm (T-209)	2.456	n/a	152.9
VMA	14.0	13 - 15	13-15	% Comp. @ Nini (8)	85.1	<89	
VFA	71.5	65-75	65-75	% Comp. @ Nmax (160)	96.8	<98	
Gse	2.663	n/a	n/a	Dust Proportions (D_p)	1.17	0.6 - 1.6	
% Effective AC (P_{be})	4.4	n/a	n/a	% Binder Absorption (P_{ba})	0.95	n/a	

PROPERTIES AT N-DESIGN (100 GYRATIONS)

Percent AC	Maximum Theoretical Unit Weight Gmm	kg/m³	lbs/ft³	Gmb as %Gmm	Bulk Density @ Ndes Gmb	kg/m³	lbs/ft³	Pbe/-200	Percent Air Voids	Percent VMA	Percent VFA
4.5	2.485	2485	154.7	93.6	2.327	2327	144.8	1.3	6.4	14.6	56.2
5.0	2.467	2467	153.6	95.3	2.350	2350	146.3	1.2	4.7	14.2	66.5
5.5	2.449	2449	152.4	96.5	2.363	2363	147.1	1.0	3.5	14.2	75.1
6.0	2.431	2431	151.3	97.7	2.375	2375	147.8	0.9	2.3	14.1	83.8

	°C	°F	Temp Band (°C)	Temp Band (°F)	Tesile Strength Ratio(AASHTO T-283)			
					Dry	Wet	TSR	Minimum Required
Mixing Temp.	169	335	166 - 171	331 - 340				
Molding Temp.	156	313	152 - 160	306 - 320	134 psi	124 psi	92.2%	80.0%
Release to Traffic Temp:		151	Max		924 kPa	855 kPa		

COMPOSITE BLEND AGGREGATE PHYSICAL PROPERTIES

Tests Performed	Design Data	Design Criteria	Tests Performed	Design Data	Design Criteria
ASTM D4791 - Flat & Elongated Pieces	14%	20% max	ASTM C 131, LA Abrasion	27%	40 max
ASTM D1252, Fine Aggregate Angularity	45.9	45 min	ASTM C 88, Soundness Loss	7.2%	15 max
ASTM D 5821, Fractured Faces	99/97	95/90	AASHTO T-90, Plastic Index	SNP	NP
ASTM D 2419, Sand Equivalent	71	45 min	Section 910, Aggregate Index	13.7	N/A
Weight for Gyratory Pucks (grams)	4,675	n/a	Daily Production Gradation Control		Plant Sample From Silo
Ignition Correction Factor	0.17	n/a			

orted By:

Tested by: Jaime Galvan Jr.
Ray Cruz
Asphalt Lab Technician

Reviewed by:
Steven A. Hooper, NM Registered Professional Engineer # 7093